 doi:10.20944/preprints202011.0292.v1

Article

Prediction of Drug Potencies of BACE1 inhibitors: A molecular Dynamics simulation and MM_GB(PB)SA Scoring

Mazen Y Hamed[1]

[1] Affiliation 1; Chemistry Department; Birzeit University; Palestine; mhamedbirzeit.edu

* Correspondence: mazen1hame@gmail.com

Abstract: Alzheimer's disease (AD) is a progressive neurodegenerative brain disorder. One of the important therapeutic approaches of AD is the inhibition of β-site APP cleaving enzyme-1 (BACE1). This enzyme plays a central role in the synthesis of the pathogenic β-amyloid peptides (Aβ) in Alzheimer's disease. A group of potent BACE1 inhibitors with known x-ray structures (PDB ID 5i3X, 5i3Y, 5iE1, 5i3V, 5i3W, 4LC7, 3TPP) were studied by molecular dynamics simulation and binding energy calculation employing MM_GB(PB)SA. The calculated binding energies gave Kd values 0.139 µM, 1.39 nM, 4.39 mM, 24.3 nM, 1.39 mM, 29.13 mM and 193.07 nM, respectively. These inhibitors showed potent inhibitory activities in enzymatic and cell assays. The K_d values were compared with experimental values, the structures were discussed in view of the energy contributions to binding. Drug likeness of these inhibitors is also discussed. Accommodation of ligands in the catalytic site of BACE1 is discussed depending on the type of fragment involved in each structure. Molecular dynamics (MD) simulations and energy studies were used to explore the recognition of the selected BACE1 inhibitors by Asp 32, Asp228 and the hydrophobic flap. The results show that selective BACE1 inhibition may be due to the formation of strong electrostatic interactions with Asp32 and Asp228 and a large number of hydrogen bonds, π-π and Van der Waals interactions with the amino acid residues located inside the catalytic cavity. Interactions with the ligands show a similar binding mode with BACE1. These results help to rationalize the design of selective BACE1 inhibitors.

Keywords: Alzheimer's disease; BACE1; Molecular dynamics; MM/GBSA ; Inhibitors; Drug likeness; Ligand efficiency, K_d.

1. Introduction

Alzheimer's disease (AD) is a progressive, neurodegenerative disease of the brain. AD and the associated dementia were connected to Amyloid plaque accumulated in the brain. The β-Site Amyloid Precursor Protein Cleaving Enzyme 1 (BACE1) is an aspartic protease enzyme fixed to the cell membrane; it acts to produce β-amyloid (Aβ) in the signaling pathways in Alzheimer's disease (AD). Excessive accumulation Aβ is believed to induce pathological changes and causes dementia in brains of AD patients.

The enzyme BACE1 initiates the cleavage of amyloid precursor protein (APP) at the β-secretase site, then Aβ is released as a result of further cleavage of the BACE1-cleaved C-terminal APP fragment[1]. Blocking BACE1 proteolytic activity will suppress Aβ generation and reduce the formation of amyloid. Research has been directed towards potent BACE1

Preprints (www.preprints.org) | NOT PEER-REVIEWED | Posted: 10 November 2020 doi:10.20944/preprints202011.0292.v1

inhibitors for AD therapy. Recent breakthroughs in developing BACE1 inhibitors which can penetrate brain cells, made the targeting of amyloid deposition-mediated pathology as a therapy more reachable. Various strategies that have successfully led to the discovery of BACE1 inhibitor drugs that have reached the stage of clinical trials.

BACE1consists of three domains: An N-terminal, a single transmembrane domain, and a cytosolic C-terminus. The catalytic ectodomain has an aspartic protease fold, with the substrate-binding cleft located between the N- and C-terminal lobes (Figure 1).

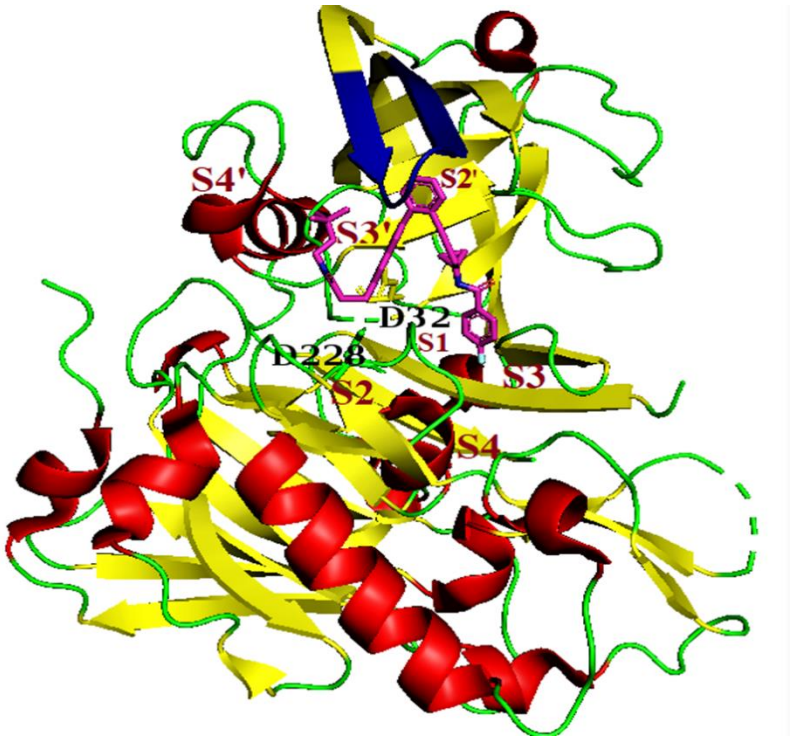

Figure 1: Structures of BACE1 in complex with inhibitor **1** (PDB ID 5i3X. The inhibitor 68J (Pink), catalytic dyad D228 and D32, flap (Blue).

The crucial catalytic aspartate (Asp) dyad, Asp32 and Asp228, is located at the interface of the two lobes[2]. A hairpin loop “flap” in the N terminal lobe partially covers the cleft in a perpendicular orientation and contains Valine 69 Tyrosine 71 and Threonine 72 (colored blue in Figure 1). The conformational changes in the flap control the substrate access to the active site. The first BACE1 substrate analogue inhibitors to mimic the APP-cleavage sequence which contain a non-cleavable peptide bond, showed high potency, but gave poor oral bioavailability and low brain penetration which prevented therapeutic utility[3][4]. Amidine containing compounds that form optimal interactions with the Asp32 and Asp228

 doi:10.20944/preprints202011.0292.v1

enhanced the search for BACE1 inhibitors[1] [2] [5]. These Asp-binding amidine and guanidine inhibitors have been studied and the cyclohexyl groups were found to bind the S1 and the lipophilic S1′ pockets (Figure 1).

Other compounds features a quaternary carbon that acts as a vector into the S1−S3 and S2′ pockets of the catalytic site (Figure 1)[6]. In other inhibitors, the basicity of the amidine/guanidine function provides a formal positive charge which impacts the optimization of physicochemical parameters. In contrast, there are a few known ligands that bind to the catalytic cleft without interacting with the Asp32 and Asp228 residues. Merck reported an inhibitor (Pyrimidine) which binds to the S1 and S3 pockets[7] and Elan Pharmaceuticals reported an S2 pocket binding inhibitor[8].

Researchers employed several methods to predict drug potency by calculating the binding free energies of potential drugs as ligands to protein targets[9][10][11]. Thermodynamic integration (TI) and free energy perturbation (FEP) have been successfully applied to calculate free energy values close to experimentally reported values[12]. These methods proved to be computationally expensive and not practical. On the other hand, docking programs were employed to obtain scores for large numbers of candidate drugs but proved to be not very accurate in predicting the free energies of inhibitor binding to potential sites on the proteins[13][14]. The approximations used in these methods such as ignoring protein flexibility, inadequate treatment of solvation and simplifying the energy functions used made them less valuable for studying drug binding. The MM/GBSA method provides faster estimates of the free energy of binding, as compared to the other computational free energy methods, such as free energy perturbation (FEP) or thermodynamic integration (TI) methods[15][16]. Comparison studies have also shown that MM/GBSA outperforms Molecular Mechanics/Poisson Boltzmann Surface Area MM/PBSA in calculating the inhibitor binding energy to protein receptors [17].The MM/GBSA method[17][18] has been widely exploited in free energy calculations and its rescoring generally yields better results than docking for the Directory of Useful Decoys, Enhanced data set [18]. MMGBSA when applied to any protein-ligand system requires the calculation of an explicit entropy

Preprints (www.preprints.org) | NOT PEER-REVIEWED | Posted: 10 November 2020 doi:10.20944/preprints202011.0292.v1

term[9][18] [19] and, for some systems, displays overly large contributions to the absolute free energy of binding[20][21].

The design of BACE1 inhibitors was concentrated on peptidic substrate transition-state mimic inhibitors; these ligands showed low nanomolar inhibition potency for BACE1, but have poor pharmacokinetic properties[1]. Recently, second-generation inhibitors were designed based on structure-based drug design. Low molecular weight molecules with excellent cell permeability like OM99-2, a substrate-based inhibitor with a highly potent BACE1 inhibition (IC50 =1.6 nM) have little peptidic character, and showed an enhanced pharmacokinetic profile. Fragment-based inhibitors discovered using a computational approach have led to designing potent small-size BACE1 inhibitors [22].

In this work, the binding energies of a group of inhibitors to BACE1 were calculated employing MD simulation and MM/GBSA. The contributing energies were analyzed and the values were correlated to experimentally found K_d values for the inhibitors. The feasibility of MM/GBSA to estimate K_d values for drugs and how to optimize drug structures in view of the results to give acceptable inhibition are discussed [23].

2.Methods

2.1 Molecular dynamics simulations

Molecular dynamics simulations were performed on the initial structures based on the x-ray crystal structure of the protein-inhibitor complexes with PDB identifications shown in Table 1. MD simulations were carried out using the Amber18.0 package[24][25] [26]on GPU accelerated version[27], employing the AMBER force field ff14SB for proteins and nucleic acids which describes the potential energy of the system[28][29]. All atom explicit water molecular dynamics simulations were performed on all systems. The PDB file was downloaded in ***pymol*** [30]**,** and the complex prepared using ***pdb4amber*** program, inspected, salt and water were removed. The receptor, ligand and complex pdb files were saved separately using text editor.

Preparing ligand, receptor and Complex files for Amber[31]**:**

Preprints (www.preprints.org) | NOT PEER-REVIEWED | Posted: 10 November 2020 doi:10.20944/preprints202011.0292.v1

Antechamber [32]package in Amber Tools[26] was used to create topology and coordinate files for the simulations of ligands, ***Antechamber*** is designed to be used with the "general AMBER force field (**GAFF**)"[32], for organic molecules. This force field has been specifically designed to cover most pharmaceutical (organic) molecules and is compatible with the traditional AMBER force fields in such a way that the two can be mixed during a simulation. Hydrogens were added to the ligand (using *reduce*) then the **ligand. frcmod** and **library** files were prepared for amber, and the **tleap** editor was used to load the complex or combine the ligand and receptor. The complexes were solvated in a **TIP3P**[33] cubic water box with water molecules extending 15Å from the complex surface to the water box boundary, Na^+ or Cl^- ions were added to neutralize the system depending on the charge. The structure of the complex was checked for errors and then converted to topology and coordinate files. The particle mesh Ewald method [34] was used for treating long range electrostatics, a 9Å cutoff was set for long range interactions. The force field energy of each structure was minimized by progressively relaxing the system before starting the MD simulations. Minimizations were performed employing steepest descent followed by conjugate gradient minimizations (1000 cycles in tandem).

After relaxation of the system it was heated to 300K applying harmonic restraint (10 Kcal/$Å^2$.mol) on solute. This was followed by an unrestrained 2ns MD simulation at 300K and 1 atm to equilibrate the system and adjust the density.

. SHAKE algorithm [35]was used to constrain hydrogen atoms in order to enable a longer time step (2fs) in the simulation. A Langevin thermostat [36][37]with 2 ps^{-1} collision frequency and weak coupling barostat with 2 ps of relaxation time were employed. Production MD simulations were carried out for 150 ns and gave converged trajectory evident in the RMSD behavior which showed good stability within 1.5Å. Trajectories were collected at 2 ps intervals. These trajectories were used to calculate the binding free energy using MMPBSA.py script[38]; 50 or 100 frames were used in the calculations. Loss in flexibility upon binding expressed as entropy change ($T\Delta S$) was calculated by normal modes using the same snapshots which were used for calculating ΔG binding. Then the absolute free energy of binding was calculated (equation 4). The binding energy of the complex was calculated using the MM/GBSA method.

Preprints (www.preprints.org) | NOT PEER-REVIEWED | Posted: 10 November 2020 doi:10.20944/preprints202011.0292.v1

2.2 The Generalized Born/Surface Area Model

The MM/PBSA and MM/GBSA methods [44][9] have been used to estimate ligand-binding affinities in many systems, giving correlation coefficients compared with experiments of r^2 in the range of 0.3 to 0.9, depending on the protein, with MM/GBSA giving better results in this case. The results strongly depend on details in the method, especially the continuum-solvation method, the charges, the dielectric constant, the sampling method and the entropies. The methods often overestimate differences between sets of ligands.

The (MM/PB(GB)SA method uses representative snapshots from an ensemble of conformations to calculate free energy change between the bound and unbound states of receptor and ligand, (equations 1A, 1B). Before using MM-GBSA[11][45][46][39] the system equilibration was verified by considering temperature, density, total energy and root mean squared deviation of coordinates (RMSD). An RMSD value relative to the crystal structure of 1.5Å was deemed acceptable. Extensive analysis of each trajectory was performed to make sure the energies calculated are reliable depending on the snapshots [50][51][52]. To estimate the total solvation free energy of a molecule, ΔGsolv, one typically assumes that it can be decomposed into the "electrostatic" and "non-electrostatic" parts

$$\Delta G_{solv} = \Delta G_{el} + \Delta G_{nonel}$$

where ΔGnonel is the free energy of solvating a molecule from which all charges have been removed (i.e. partial charges of every atom are set to zero), and ΔGel is the free energy after removing all charges in vacuum, and then adding them back in the presence of a continuum solvent environment. Generally speaking, ΔGnonel comes from the combined effect of two types of interaction: the favorable van der Waals attraction between the solute and solvent molecules, and the unfavorable cost of breaking the structure of the solvent (water) around the solute. In the current Amber codes, this is taken to be proportional to the total solvent accessible surface area (SA) of the molecule, with a proportionality

Preprints (www.preprints.org) | NOT PEER-REVIEWED | Posted: 10 November 2020 doi:10.20944/preprints202011.0292.v1

constant derived from experimental solvation energies of small non-polar molecules, and uses a fast LCPO algorithm to compute an analytical approximation to the solvent accessible area of the molecule. Within Amber GB models, each atom in a molecule is represented as a sphere of radius Ri with a charge qi at its center; the interior of the atom is assumed to be filled uniformly with a material of dielectric constant 1. The molecule is surrounded by a solvent of a high dielectric constant 80 for water at 300 K) (Equation 2). The GB model approximates ΔGel while the nonpolar energy is usually estimated using the solvent-accessible surface area (SASA) (Equation 6) [9] [47]

ΔG bind = G_{RL} -G_{R} -G_{L} where R = receptor, L= Ligand (1A)

$$\Delta G^{0}_{bind,\,solv} = \Delta G^{0}_{bind,\,vacuum} + \Delta G^{0}_{solv,\,complex} - (\Delta G^{0}_{solv,\,ligand} + \Delta G^{0}_{solv,\,receptor}) \quad (1B)$$

$$\Delta G^{0}_{solv} = G^{0}_{electrostatic,\,\epsilon=80} - G^{0}_{electrostatic,\,\epsilon=1} + \Delta G^{0}_{hydrophobic}$$

(2)

$$\Delta G^{0}_{vacuum} = \Delta E^{0}_{molecular\ mechanics} - T \cdot \Delta S^{0}_{normal\ mode\ analysis}$$

(3)

$\Delta G = \Delta H - T\Delta S = \Delta E_{MM} + \Delta G_{SOL} - T\Delta S$ (4)

$\Delta E_{MM} = \Delta E_{internal} + \Delta E_{electrostatic} + \Delta E_{vdw}$ (5)

$\Delta G_{SOL(PB/GB)} = \Delta G_{PB/GB} + \Delta G_{SA(PB/GB)}$ (6)

where ΔE_{MM} is total gas phase energy (sum of $\Delta E_{internal}$ + $\Delta E_{electrostatic}$ + ΔE_{vdw}). $\Delta G_{SOL(PB/GB)}$ is sum of nonpolar and polar contributions to solvation calculated by PB or GB. $T\Delta S$ is conformational entropy upon binding computed by normal- mode analysis on a set of conformational snapshots taken from MD simulations. $\Delta E_{internal}$ is internal energy arising from bond, angle, and dihedral terms in the MM force field. $\Delta E_{electrostatic}$ is electrostatic energy as calculated by the molecular mechanics (MM) force field. ΔE_{vdw} is van der waals contribution from MM. $\Delta G_{PB/GB}$ is nonpolar contribution to the solvation free energy calculated by an empirical model. The nonpolar solvation free energy is typically given by

Preprints (www.preprints.org) | NOT PEER-REVIEWED | Posted: 10 November 2020 doi:10.20944/preprints202011.0292.v1

an empirical formula that is proportional to the solvent accessible surface area of the solute: $\Delta G_{SA}=\gamma \cdot SASA + b$, where γ is the surface tension constant and b is a correction constant ($\gamma = 0.00542$ kcal·mol^{-1}·Å^{-2} and b = 0.92 kcal/mol in the AMBER package). $\Delta G_{SA/GB}$ is the electrostatic contribution to the solvation free energy calculated by the PB or GB method, respectively.

One-thousand 2 ps spaced snapshots of each complex were generated from the MD trajectories, and all water molecules and counter-ions were removed before MM-PBSA/GBSA calculations. Coordinates were extracted by using the *extract-coords.mmpbsa*" script and the ΔG values were calculated by using the "MMPBSA.py" script[38].

3. **Results and discussion**

3.1 Data analysis

The RMSDs, dynamic cross-correlation analysis, principal component analysis (PCA), were processed using the CPPTRAJ module in Amber 18 package [42]. The principal component analysis (PCA) was performed to help in sampling [44][45]

System stability under MD simulations (see Figure 2 a, b, c and d)

Preprints (www.preprints.org) | NOT PEER-REVIEWED | Posted: 10 November 2020 doi:10.20944/preprints202011.0292.v1

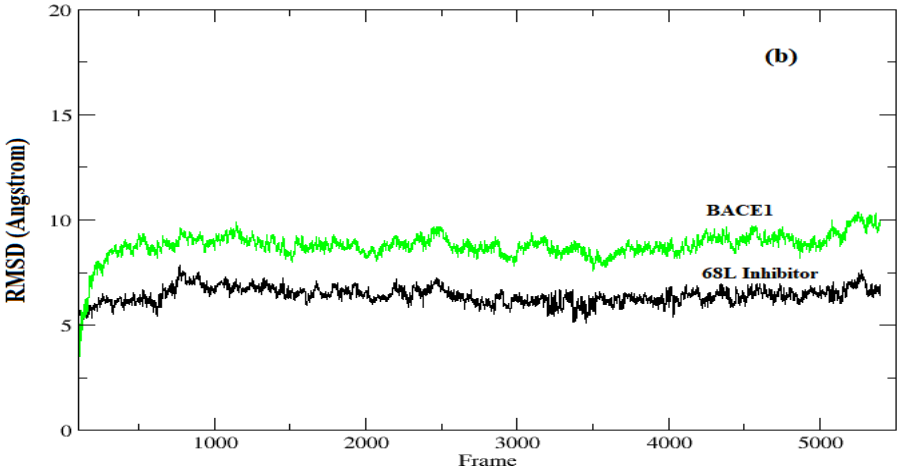

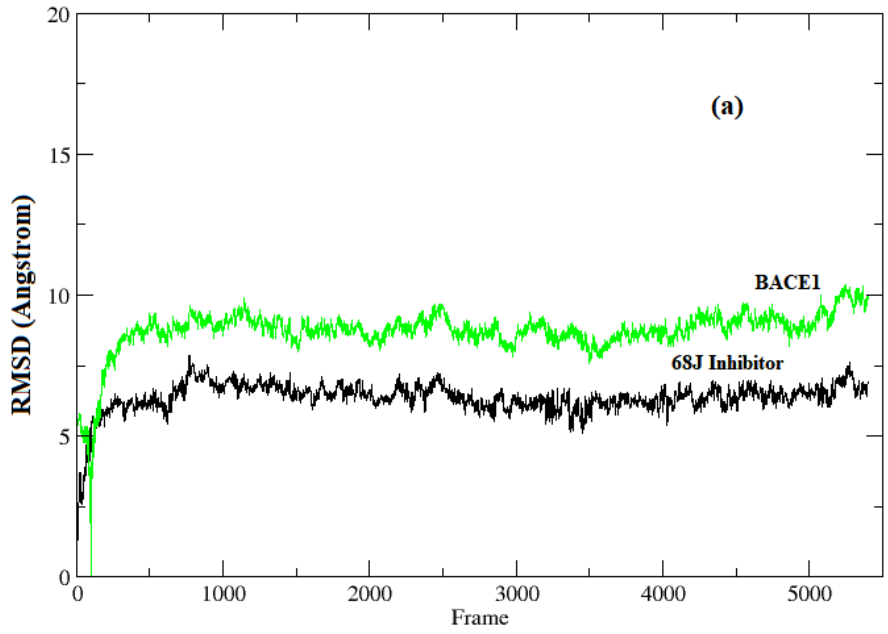

Preprints (www.preprints.org) | NOT PEER-REVIEWED | Posted: 10 November 2020 doi:10.20944/preprints202011.0292.v1

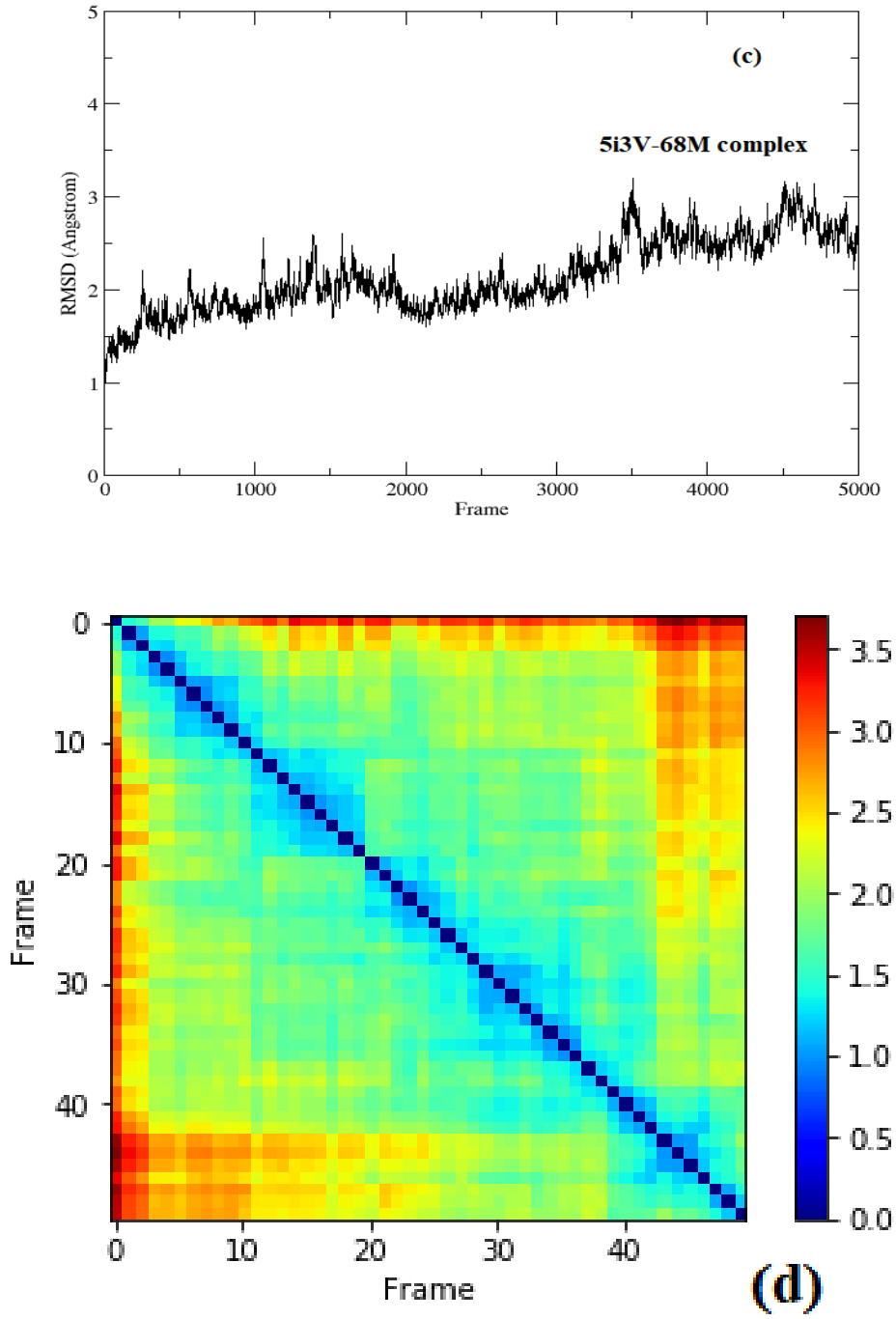

Figure 2: RMSD evolutions from MD simulations of (a) BACE1 (Green) and Inhibitor 68J (black) in 5i3X; (b) 5i3W BACE1 (green) and 68L inhibitor (black); (c) 5i3V the BACE1-68M complex (d): pairwise plot of RMSD of BACE1-68J complex in 5i3X, RMSD pairwise computed for first 5000 snapshots and skip every 10 frames.

Before starting MD analysis, the root-mean square deviation (RMSD) evolution of the protein backbone Cα for each complex was monitored throughout the 200 ns MD simulations to ensure stability of the systems. As shown in Figure 2, the RMSD evolution

 doi:10.20944/preprints202011.0292.v1

for Cα of BACE1 bound with inhibitors exhibited relatively small fluctuations at the start of simulation, then was stable and changes were within 1.0 Å. Accordingly, the RMSD evolution of the heavy atoms of the inhibitors, maintained relative stability (RMSD fluctuation <1 Å) during the 200 ns simulation. Pairwise RMSD for specific snapshots was Computed using *pytraj* in Amber. The RMSD to the experimental structure reference was computed, then, pairwise RMSD for first 5000 snapshots and skipping every 10 frames was computed (Figure 2(d)).

.

Preprints (www.preprints.org) | NOT PEER-REVIEWED | Posted: 10 November 2020 doi:10.20944/preprints202011.0292.v1

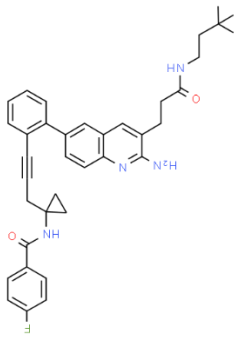

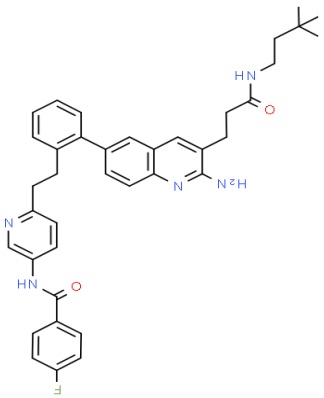

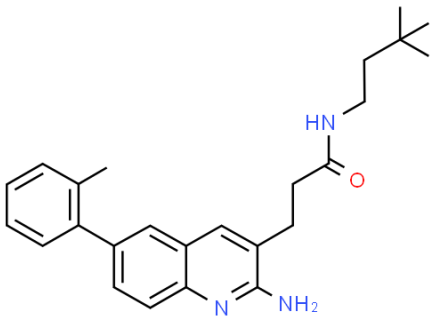

(1) 5i3X-68J **(2) 5i3Y-68K** **(3) 5iE1-6BS**

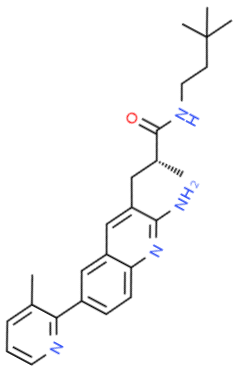

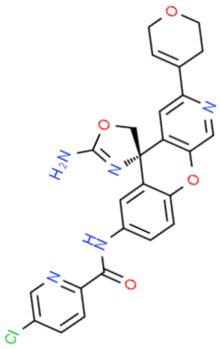

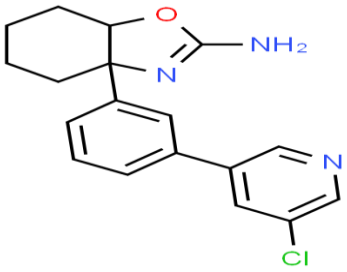

(4) 5i3V-68M **(5) 5i3W-68L** **(6) 4LC7-1WP**

Preprints (www.preprints.org) | NOT PEER-REVIEWED | Posted: 10 November 2020 doi:10.20944/preprints202011.0292.v1

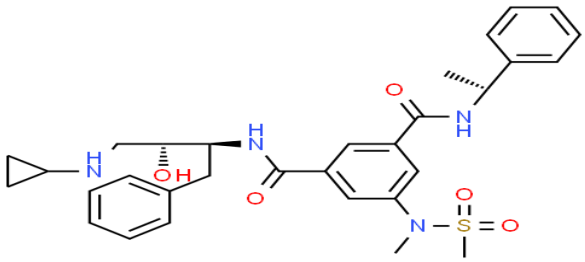

(7) 3TPP-5HA

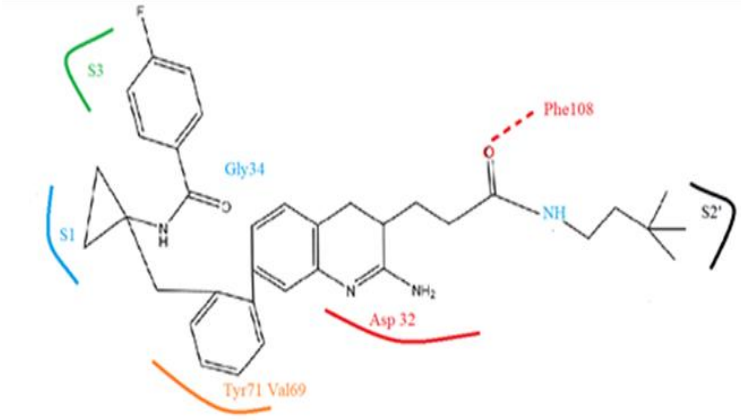

(8) binding sites of 68J inhibitor

Figure 3: structures1 to 7 are selected BACE1 inhibitors with their PDB ID. Structure (8) shows the binding mode of inhibitors derived from MD simulation using 68J as an example.

3.2 Prediction of binding mode and key interactions of Inhibitors to BACE1

MD simulations were performed to elucidate the key interactions of inhibitors responsible for inhibitory activity against β-amyloid (Aβ) accumulation. The MD simulations were performed to evaluate the favored binding modes and key interactions of BACE1 with various inhibitors (Figure3 and Figures 6 and 8).

Preprints (www.preprints.org) | NOT PEER-REVIEWED | Posted: 10 November 2020 doi:10.20944/preprints202011.0292.v1

Table 1: The calculated energies of BACE1 Inhibitors

PDB id -inhibitor	$K_{d\ Exp}$ [46][47]	IC_{50} [46][47]	ΔH_{GBSA} kcal/mol	$T\Delta S$	$\Delta G_{binding\ Calculated}$ kcal/mol	ΔG_{exp}	K_d from calculated ΔG_{bind}**
5i3x- (1)	8 nM , 0.8nM	191 nM, 9nM	-44.5(4)	-25.2(5)	-19.3(5)	-11.34	0.000139 nM
5i3y-(2)	0.4000 nM	16nM, 0.8nM	-37.4(3)	-24.96(6)	-12.4(7)	-13.16	1.39 nM
5ie1-(3)	140 nM	140nM	-30.5(3)	-22.98(6.2)	-7.5 (6)	-9.60	4.39 mM
5i3w-(5)	0.6nM		-32.2(2.6)	-24(4)	-8.15 (4)	-12.9	1.39 mM
5i3v-(4)	16 nM	16 nM, 35 nM	-32.92(5.2)	-22.26(4)	-10.66(4)	-10.92	24.3 nM
3tpp-(6)	233 nM	15 nM, 15nM	-35.6(6)	-26.21(5)	-9.4 (4)	-9.28	193.07nM
4lc7 –(7)		11800 nM, 14nM	-24.64(5)	-22.5(5)	-2.15 (5)	-6.8	29.13 mM

** $\Delta G = RT ln K_d = 1.4 log K_d$ (K_d in $mol.L^{-1}$)

The Binding energies of inhibitors with BACE1 are shown in Tables 1 and 2 and in Figures 4 and 5; inhibitors under study bind Asp32 and Asp228 (Tables 4 and 5) and Figures 6 and 9, except for 4LC7 which binds Asp93 and Asp289 (see Figure 9G).

Preprints (www.preprints.org) | NOT PEER-REVIEWED | Posted: 10 November 2020 doi:10.20944/preprints202011.0292.v1

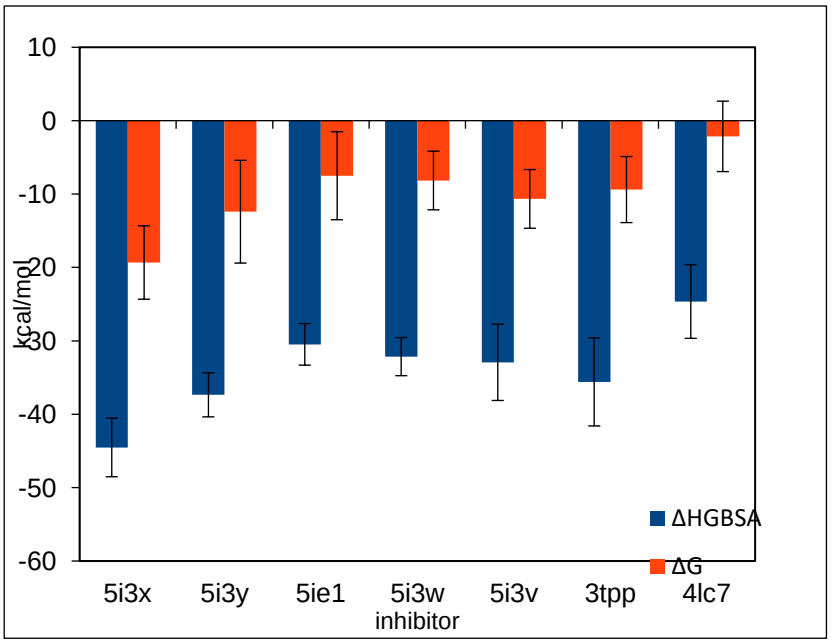

Figure 4: The binding Energies of Inhibitors calculated by MM/GBSA

Table 2: The different components of binding free energy (kcal/mol) between Inhibitors-BACE1 complex evaluated using the MM–GBSA method.

Number (Figure 2)	PDB ID	vdw	E EL	E GB	E surf	E solv	ΔH_{GBSA}
1	**5i3x**	-67.1(3.1)	-26.99(6.1)	58.3(4.9)	-8.72(0.24)	49.6(4.83)	-44.52(4)
2	**5i3y**	-59.13(3.4)	-16.8(3.4)	45.8(4.2)	-7.2(0.5)	38.6(3.8)	-37.36(3)
3	**5ie1**	-39.15(2.96)	-36.21(2.9)	50.77(1.5)	3.76(0.02)	44.9(0.7)	-30.48(2.8)
4	**5i3v**	-43.69(3.4)	-21.62(7.7)	38(5.6)	-5.6(0.52)	32.4(5.4)	-32.92(5.2)
5	**5i3w**	-55.34(2.86)	-14.12(3.1)	44.1(2.6)	-6.8(0.19)	37.3(2.5)	-32.15(2.6)
6	**4lc7**	-34.04(2.9)	-13.2(13)	26.8(11)	-4.3(0.3)	22.6(10.9)	-24.64(5.02)
7	**3ttp**	-10.73(0.9)	-66.97(1.9)	-55.9(1)	5.6(0.03)	-40.26(1.02)	-35.6(6)

Preprints (www.preprints.org) | NOT PEER-REVIEWED | Posted: 10 November 2020 doi:10.20944/preprints202011.0292.v1

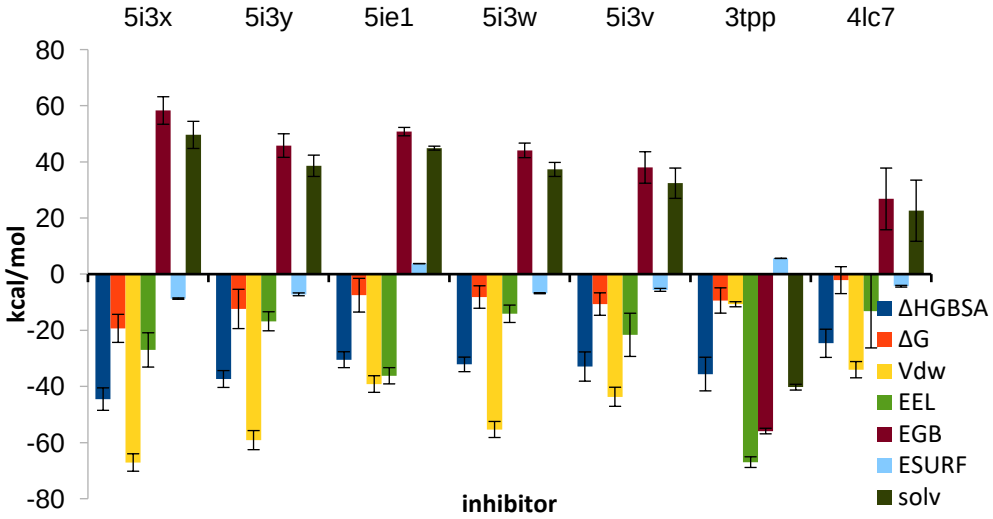

Figure5: The breakout of binding energy ΔH to its contributing energies for inhibitors under study.

The flap, a β-hairpin loop containing residues Tyr71to Val69, positioned directly over the catalytic dyad, can open and close to allow substrate and inhibitor access to the active site Figure1 and 6.

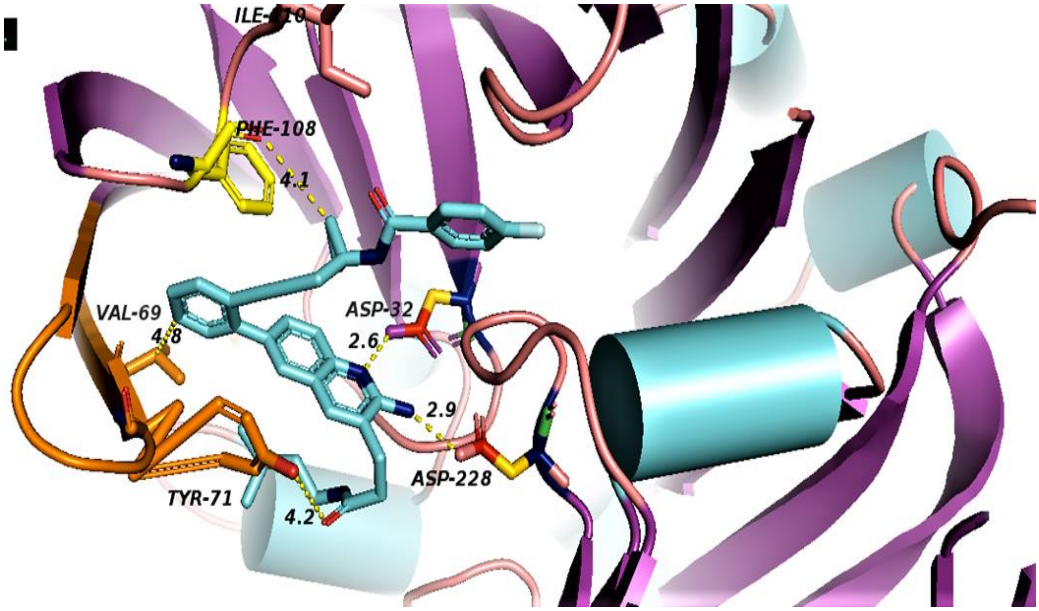

Figure 6: A) structures of BACE1 complexed with 1(shown in cyan), it shows the distances of the residues from inhibitor **1** in 5i3X, The aspartate pocket (Asp32 and Asp228); the flap shown in orange which contains Val69, Tyr 71. Distances are listed in Table 3. [for views

Preprints (www.preprints.org) | NOT PEER-REVIEWED | Posted: 10 November 2020 doi:10.20944/preprints202011.0292.v1

of inhibitors binding to BACE1 see Figures 1-s to 8-S]

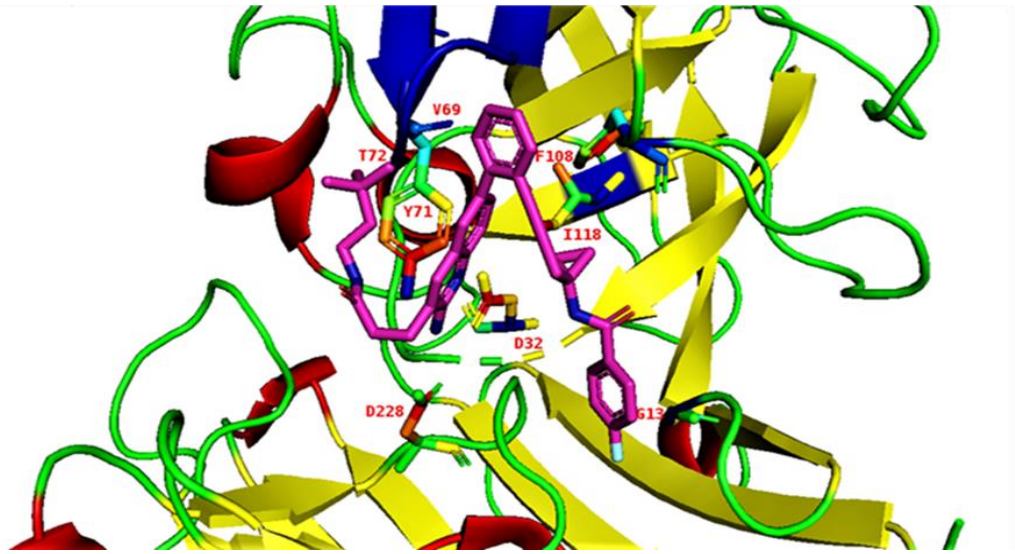

Figure6: B) The binding pocket of BACE1; inhibitor 1 in 5i3X is shown (pink) and all potential binding residues labeled, the flap shown in blue. structure of BACE1 complexed with inhibitor 1 (shown in pink), interactions between ligand and protein at the catalytic aspartic acids Asp32 and Asp228 and at Trp72 of the S2'region (Table 3).

Table 3: some bond distances measured in the average structure using pymol

Inhibitor		ASP32 Oxygen Å	ASP228 oxygen Å	Gly 13 Å	Ser35 Å	Hydrophobic: Tyr71 Å	Hydrph:Val69 Å
5i3X	N of pyridine ring	2.6, 3. 6	4.9, 5.1			3.0 to 3.9	4.0 – 4.9
	NH2	2.9, 3.6	2.9, 3.0				
5i3Y	N of pyridine ring	3.5	5.0, 5.2	3.8	4.1-5	4.2- 4.3	3.9-4.4
	NH2	2.6	3.0, 3.1				

Preprints (www.preprints.org) | NOT PEER-REVIEWED | Posted: 10 November 2020 doi:10.20944/preprints202011.0292.v1

3TPP		2.7, 3.5	2.7, 3.9	3.4 Gly230: 3.1		Gln 73: 3.2	
4LC7		Asp93: 2.7, 2.7	Asp289: 2.8, 2.8	Leu91: 4.3	Tyr132: 3.6		

All inhibitors occupy similar binding pockets and more importantly form hydrogen bond interactions with the catalytic dyad of Asp32 and Asp228. The active site of BACE1 is mostly hydrophobic, with no charged residues within 8 Å distance of Asp dyad; the Aspartate residues form bonds with the amine and the nitrogen of the pyridine ring Figure 1 structure 8 and Figure 8.

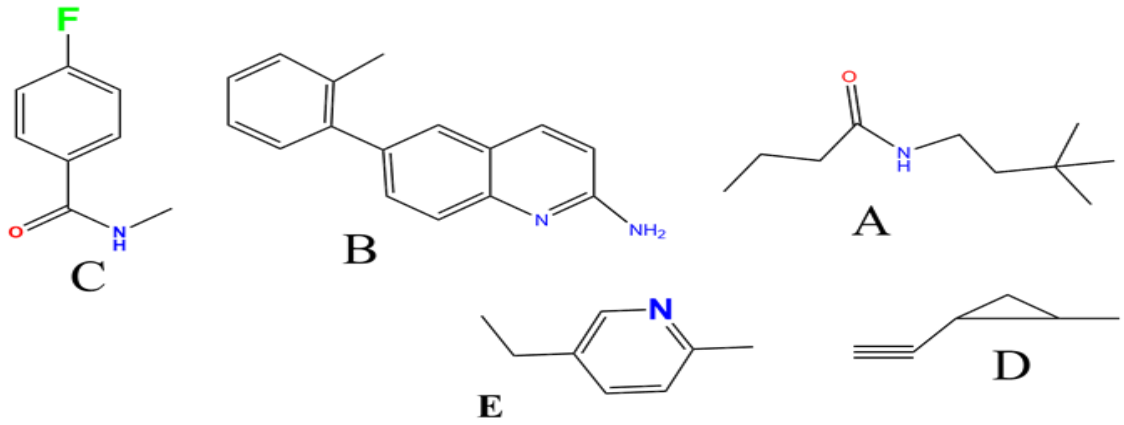

Figure 7: Structure of the fragments in Inhibitors 1,2,3 and 4

The hydrophobic interactions Tyr71, Val69, Gly13. Gly230. Phe108, Leu30 and Ile118 are common in all 68J, 68K, 68L and 68M inhibitors, all display hydrophobic contacts with residues The nitrogen containing heterocycles are often referred to as the aspartyl binding motif see Figure 8 shown below

Preprints (www.preprints.org) | NOT PEER-REVIEWED | Posted: 10 November 2020 doi:10.20944/preprints202011.0292.v1

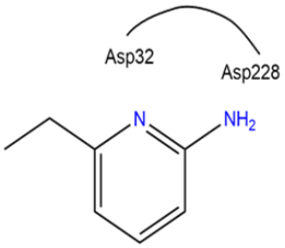

2-Aminopyridine

Figure 8: binding of Asp32 and Asp228 to the 2-aminopyridine moiety.

Inhibitors 1,2,3 and 4 share fragments A and B in Figure 7, where the terminal CR3 forms hydrophobic interactions in S_2' pocket which contains D228. The correlation coefficient of binding energy (ΔH) for these 4 inhibitors with Vdw energy is 0.95 and $E_{surface}$ is 0.63. The 2-aminopyridine fragment forms hydrogen bonds with Asp32 (2.6Å) and a weaker interaction with Asp 228 (4.9 Å).

Table 4: Correlation coefficients (R^2) of ΔH with contributing energies (from Table II) for groups of inhibitors

Inhibitors number(from Figure 2)	vdw	E EL electrostatic	E GB polar	E surf Surface area	E solv desolvation
1,2,3,4	0.95	0.1	0.41	0.63	0.29
1,2,3,4,5	0.76	0.01	0.43	0.44	0.33
1,2,3,4,5,6	0.85	0.075	0.68	0.29	0.62
1,2,3,4,5,6,7	0.23	0.05	0.01	0.1	0.011

The correlation with electrostatic energy is very small (Table 4) indicating a mostly hydrophobic interaction on this side. The phenyl rings in structure B (Figure 7) bind Tyr 71 (3.0 Å) and Val69 (4.0 Å). Inhibitors 1 and 2 have an extra fragment C which binds the S3 pocket and differ by one fragment (where fragment D is in inhibitor 1 and replaced by fragment E in inhibitor 2) which binds S1 pocket and Gly34, where in inhibitor 1 its D and in inhibitor 2 its E. Fragment D in Figure 7 with its Л cloud gives stronger interaction than E. All differences arise from different vdw interactions, the π–π stacking interaction between the phenyl-imino group and Phe108 added stability with the enzyme

Preprints (www.preprints.org) | NOT PEER-REVIEWED | Posted: 10 November 2020 doi:10.20944/preprints202011.0292.v1

5i3W-68L (inhibitor 5) binds Asp 32, Asp 228, Gly230, Tyr71, Leu30, and Gly13, See Figure 9E. This inhibitor shares fragment C in Figure 7 with inhibitors 1-4 which binds S1 and gave an experimental ΔG value -12.5 kcal/mol and comparable vdw energy to other inhibitors1-4, while the calculated value is -8.15(4) kcal/mol . The fragment

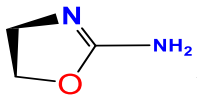

binds Asp32 and Leu30. The attachment of the phenyl ring could lead to a significant hydrophobic interaction, which would increase the probability of permeability into the brain. Thus, many BACE1 inhibitors were designed using phenyl -based analogs.

In BACE1 bound to inhibitor 7 (4LC7), shown in Figure 6(G), the heterocyclic pentatomic ring

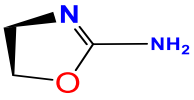

binds Asp93 and Asp289. This feature is shared with 5i3W (Figure 9(E)) in which the same ring binds Asp32 and Asp228. 5i3W (Inhibitor 5) has an extra phenyl group that binds the hydrophobic pocket (near Tyr71) which enhanced its binding over 4LC7. Inhibitor 6 (3TPP) has a different structure but shares an aryl ring with other inhibitors and it showed enhanced binding (figure 6(F). The sulfate group binds Asn233 and the attached aryl group interacts with Gln73, the fragment

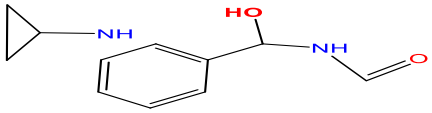

cyclopropane ring-NH binds the other end of Asn233 and Thr231. The Asp 32, Asp 228, Gly230, Gly34 and the other side of Thr231 all make hydrogen bonds with the oxygen and nitrogen on the polar end (Figure 9F).

Preprints (www.preprints.org) | NOT PEER-REVIEWED | Posted: 10 November 2020 doi:10.20944/preprints202011.0292.v1

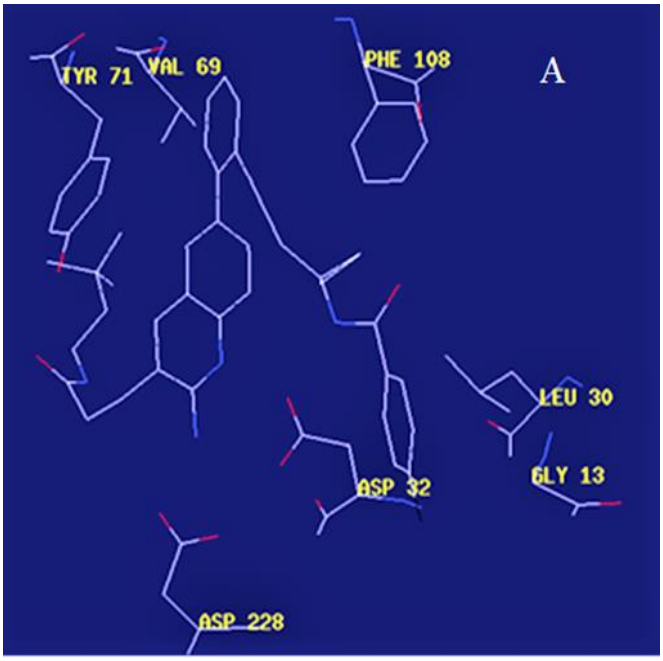

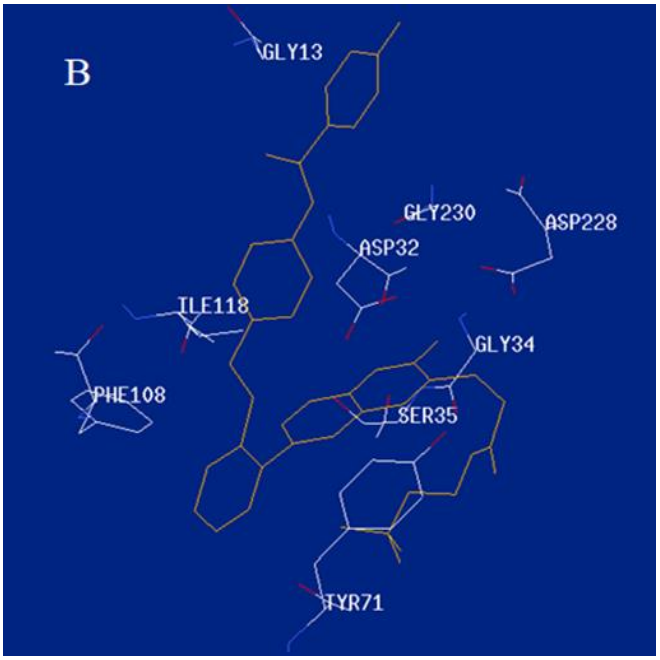

(A) 5i3X-68J (1) (B) 5i3Y-68K (2)

Preprints (www.preprints.org) | NOT PEER-REVIEWED | Posted: 10 November 2020 doi:10.20944/preprints202011.0292.v1

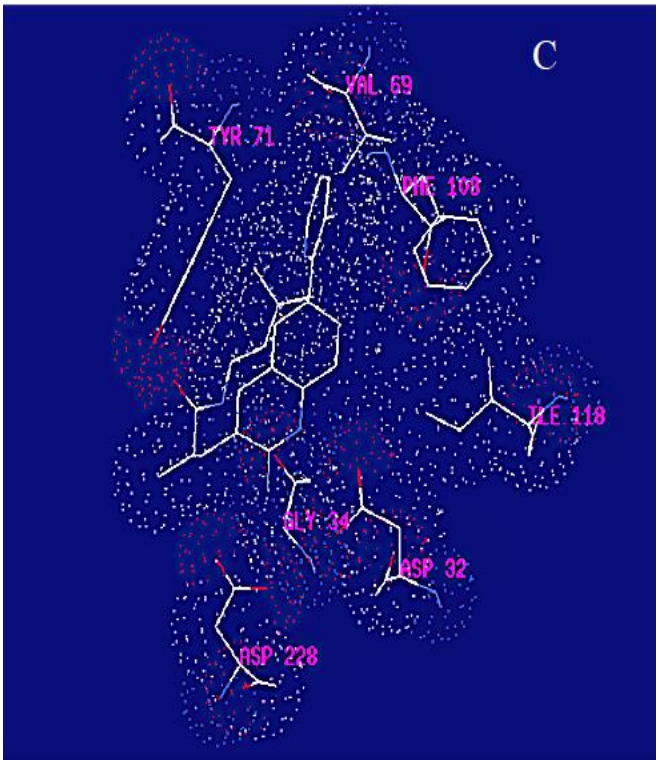

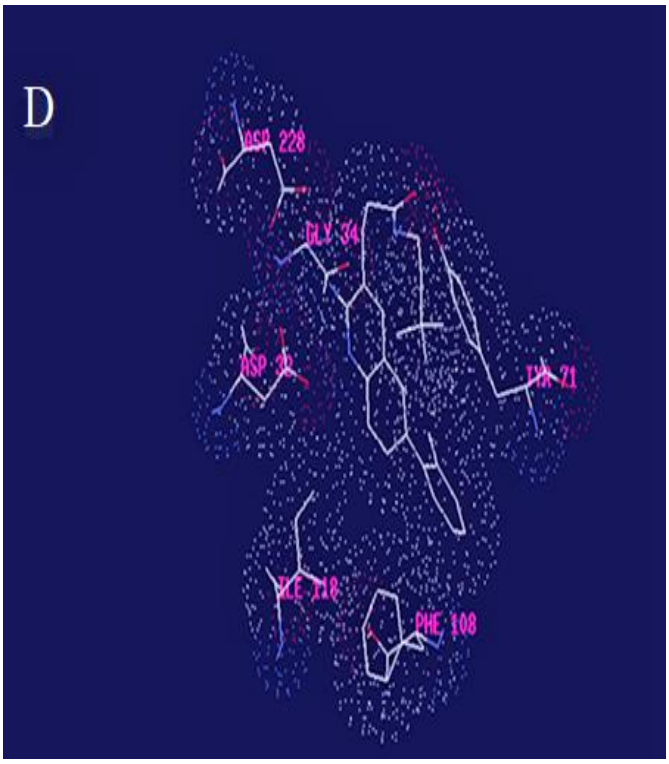

(C) 5i3V-68M (4)

(D) 5ie1- 6BS (3)

Preprints (www.preprints.org) | NOT PEER-REVIEWED | Posted: 10 November 2020 doi:10.20944/preprints202011.0292.v1

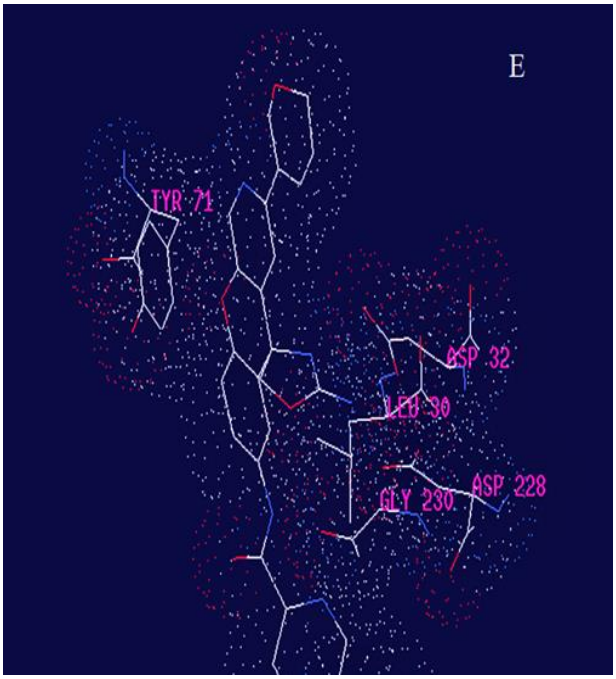

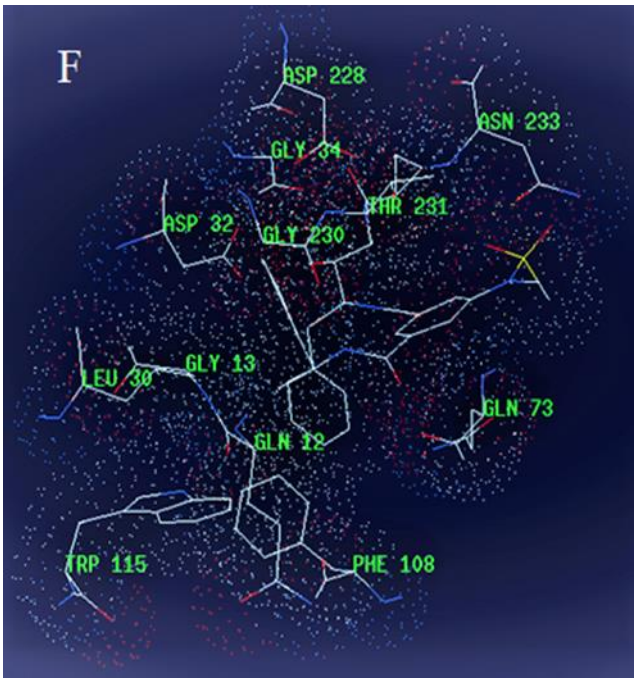

(E)5i3W-68L (5)

(F)3tpp-5HA (7)

Preprints (www.preprints.org) | NOT PEER-REVIEWED | Posted: 10 November 2020 doi:10.20944/preprints202011.0292.v1

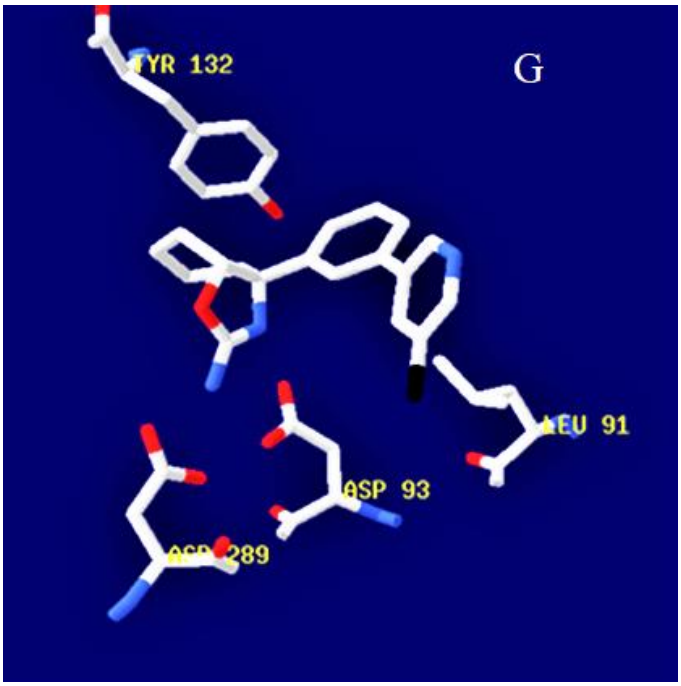

(G)4lc7 -1WP (6)

Figure 8: binding of inhibitors to BACE1obtained from average structures after MD simulation using SPDV software. Structures are defined by their PDB ID of complexes of BACE1 and Inhibitor: (a) 5i3X-68J (1); (b) 5i3Y-68K (2); (c) 5i3V-69M (4); (d) 5ie1-6BS (3); (e) 5i3W-68L (5); (f) 3TPP-5HA (7); (g) 4LC7=1WP (6). [Inhibitor numbers in brackets from Figure 2]**, see also Figures 1-s to 8-S**

Preprints (www.preprints.org) | NOT PEER-REVIEWED | Posted: 10 November 2020 doi:10.20944/preprints202011.0292.v1

Table 5: Details of Binding of inhibitors to BACE1 extracted from average structures

Protein-Inhibitor complex PDB code[48]	**ΔH Kcal/mol**	**Inhibitor**	Binding sites to the protein
5i3x I= 68J	**-44.5**	**N-(1-{3-[2-(2-amino-3-{3-[(3,3-dimethylbutyl)amino]-3-oxopropyl} quinolin-6-yl)phenyl]prop-2-yn-1-yl}cyclopropyl)-4-fluorobenzamide**	N-O:Asp228, Asp32, Gly13 Hydrph:Tyr71, Val69, Ile118, Leu30, Phe108
5i3y I= 68K	**-37.4**	**N-(6-{2-[2-(2-amino-3-{3-[(3,3-dimethylbutyl)amino] -3-oxopropyl}quinolin-6-yl)phenyl]ethyl}pyridin-3-yl)-4-fluorobenzamide**	N-O:Asp 228, Asp32, Gly34, Gly230 Hydrph:Gly13, Ser35, Tyr71, Val69, Ile118, Phe108
5i3v I= 68M	-32.9	**(2R)-3-[2-amino-6-(3-methylpyridin-2-yl)quinolin-3-yl] -N-(3,3-dimethylbutyl)-2-methylpropanamide**	N(L)-O(rec):Asp228, Asp32, Gly34, Hydrph:Tyr71, Phe108
5i3w I= 68L	-32.15	**N-[(5S)-2'-amino-3-(5,6-dihydro-2H-pyran-3-yl)-5'H -spiro[1-benzopyrano[2,3-c]pyridine-5,4'-[1,3]oxazol]-7-yl]-5-chloropyridine-2-carboxamide** C_{25} H_{20} Cl N_5 O_4	Asp 32, Asp 228, Gly 230, Tyr 71 Leu 30, Gly 13
5ie1 6BS	-30.5	**3-[2-amino-6-(2-methylphenyl)quinolin-3-yl]-N-(3,3-dimethylbutyl)propanamide**	N-O:Asp228, Asp32, Gly34 Hydrph:Tyr71, Val69, Ile118, Leu30, Phe108
3tpp 5HA	-35.6	**N-[(1S,2R)-1-BENZYL-3-(CYCLOPROPYLAMINO)-2-HYDROXYPROPYL]-5-[METHYL(METHYLSULFONYL)AMINO] -N'-[(1R)-1-PHENYLETHYL]ISOPHTHALAMIDE** C_{31} H_{38} N_4 O_5 S	Asp 32, Asp 228 Gln 73 Phe 108, Gly 34 Asn 233 Gly 230, , Leu 30 Trp 115, Thr231Gly230, Gln12 Thr232 Gly 13
4lc7 1WP	-24.64	(3aR,7aR)-3a-[3-(5-chloropyridin-3-yl) phenyl]-3a,4,5,6,7,7a-hexahydro-1,3-benzoxazol-2-amine	Asp93, Asp289, Tyr 132 Leu 91

Preprints (www.preprints.org) | NOT PEER-REVIEWED | Posted: 10 November 2020 doi:10.20944/preprints202011.0292.v1

The aryl group on the opposite end makes hydrophobic interactions with Phe108, Gly13, Gln12 and Leu30. The oxygen of the peptide bond also interacts with Gln73. The sulfate fragment in 3TPP-5HA binds S2 as seen structure below

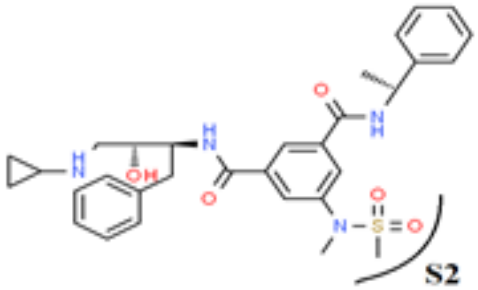

3.3 Drug likeness

Lipinski's rule of five was used evaluate drug likeness or determine if a compound with a certain pharmacological activity has properties that would make it a likely orally active drug in humans (Table 8).

Preprints (www.preprints.org) | NOT PEER-REVIEWED | Posted: 10 November 2020 doi:10.20944/preprints202011.0292.v1

PDB ID-inhibitor	M.Wt <500	LogP <5	PSA Å^2 [47]	No. H bond acceptor atoms < 5	No. H-bond donor atoms <5	N&O <10	Number of Rotatable bonds	No. rings >3
5i3x-68J	590.730	7.16** 8.18^{++}	97.11	3	3	6	13	5
5i3y-68K	617.55	7.18** 8.59^{++}	110	3	4	7	14	5
5i3v-68M	404.548	4.96** 5.89^{++}	80.9	2	3	5	8	3
5i3w-68L	488.902	2.77** 4.43^{++}	122.56	1	3	9	4	6
5ie1-6BS	389.533	5.42** 6.25^{++}	68.01	2	2	4	8	3
4lc7-1WP	328.122	3.88** 4.23^{++}	62.11	1	0	4	2	4
3tpp-5HA	597.730	3.6** 3.86^{++}	140.8	4	5	9	16	4

Table 6: Drug likeness parameters for inhibitors under study (All rules are included)

**Computed with XLOGP3 ++Computed with Open Babel

The rule was based on the observation that most orally administered drugs are relatively small and moderately lipophilic. The rule predicts the absorption, distribution, metabolism and excretion of the compound. Lipinski's rule states that, in general, an orally active drug has no more than one violation of the following criteria;

-No more than 5 hydrogen bond donors (total H_N, H_O bonds)

-No more than 10 hydrogen bond acceptors (all N+O atoms)

-Molecular mass less than 500

 doi:10.20944/preprints202011.0292.v1

-LogP less than 5 (octanol-water partition coefficient)

-Drug likeness improved LogP (-0.4 to 5.6), molecular weight 180 to 480, Total atoms 20 to 70 including N and O, Veber's Rule:

Good oral bioavailability, questioned the 500 molecular weight cutoff. Introduced PSA Polar surface area, no greater than 140 $Å^2$, and 10 rotatable bonds or less (Table 6). PSA is a commonly used metric for the optimization of a drug's ability to permeate cells[49]. Molecules with a polar surface area of greater than 140 $Å^2$ tend to be poor at permeating cell membranes. For molecules to penetrate the blood-brain a PSA less than 90 $Å^2$ is usually needed[49] . Inspecting the properties of the 7 inhibitors used (Table 8), all seven inhibitors can be suitable drugs.

Preprints (www.preprints.org) | NOT PEER-REVIEWED | Posted: 10 November 2020 doi:10.20944/preprints202011.0292.v1

Table 7: The areas of hydrophobic pockets in BACE1 for each inhibitor binding [Figure 5-S]. The calculated energies resulting from hydrophobicity using the formula -25 cal/ Å^{2}of surface area and comparing the estimated hydrophobic energy with that resulted from reported PSA[46] [50]

Proteins in Figures 5-S Pockets found by spdv software	Hydrophobic pocket area Å^2, Volume Å^3	Hydrophobic E= -25x S.A (Å^2) kcal/mol	PSA (Å^2)	Estimated Hydrophobic Energy -25xPSA kcal/mol
5i3x Bound CR3	106, 61			
	105, 75	-2.63	97.11	-2.42
	90, 72			
	71, 45			
5i3y	93, 64			
Bound t CR3	87, 57	-2.18	110	-2.75
	74, 48			
5ie1				
CR3, Hexane ring	96, 71	-2.42	68.1	-1.7
	82,55			
	67, 33			
5i3v	126, 107			
Bound CR3	61, 37	-1.54	80.9	-2.03
	58, 33			
	55, 31			
3TPP no hyd	115, 71		140.8	
No hyd	74, 47	0.0		
No hyd	59, 35			
4lc7	165 , 101			
Hexane ring	100, 61	-2.52	62.11	
	89, 60			
5i3w	80,39			
Close to ring	61,35	-1.54	122.56	-3.06
	61, 36			
	56,33			

Preprints (www.preprints.org) | NOT PEER-REVIEWED | Posted: 10 November 2020 doi:10.20944/preprints202011.0292.v1

Inhibitors 1,2,3 and 4 , which share hydrophobic mioty (Figure 7) and the 2-aminopyridine fragment (Figure 7) in their structure,showed the best correlation with PSA with binding energy(ΔH), Evdw,

E surface and E electrostatic Table 4 .

And the vdw energy showed best correlation with PSA for these inhibitors. Inhibitors. 1 to 6 showed best correlation with surface area energy. When structure 5 was added to the group, the correlation of PSA with E electrostatic improved due to the presence of hydrogen bond donors and acceptors in inhibitor 5 but to correlation with Esurface was not changedmantaing. .Analysis of energies involved in binding of inhibitors to BACE1 will aid the design of new inhibitors with more efficacy. Ligand efficiency[51][52][53] is calculated by scaling affinity by molecular size (Table 9). LE was introduced as a metric for the molecular structure to normalize the affinity with respect to molecular size by scaling the standard free energy of binding (ΔG°) with the number of heavy atoms (N_{nH}), using the formula:

$$LE\ (T, P, C) = - \Delta G/N_{nh}.$$

Preprints (www.preprints.org) | NOT PEER-REVIEWED | Posted: 10 November 2020 doi:10.20944/preprints202011.0292.v1

Table 8: Correlation coeffecients of Polar surface are with each energy contribution for various inhibitors.

Inhibitor	PSA/ΔH	PSA/E vdw	PSA/E_{GB}	PSA/E_{EL}	PSA/$E_{surface}$	PSA/E solv
1,2,3,4,5,6,7	0.23	0.23	0.32	0.24	0.014	0.31
1,2,3,4,5,6	0.3	0.14	0.17	0.14	0.4	0.13
1,2,3,4,5	0.07	0.5	0.006	0.76	0.54	0.03
1,2,3,4	0.5	0.8	0.02	0.64	0.69	0.003

LE values vary with conditions, a value of 0.3 or higher is considered favorable. LE decreases with increasing the number of heavy atoms. There is no obvious trend followed in the inhibitors in this work due to variation in structure. This variation results in high energy cost for desolvation of ligands depending on charges which took place. Ligand efficiency values of inhibitors were in the range of 0.09 to 0.41 (Table 9).

Table 9: Ligand efficiency (LE) and a comparison of ΔG experimental with the calculated ΔG values from MM/GBSA

PDB ID-inhibitor number (from Figure 2)	Nnh	LE = -$\Delta G/N_{nh}$ kcal/mol /heavy atom	ΔG_{bind} Calculated	ΔG exp
5i3X-(1)	44	0.41	-19.3	-11.34
5i3Y-(2)	47	0.27	-12.4(7)	-13.16
5iE1-(3)	29	0.26	-7.5 (6)	-9.60
5i3V-(4)	30	0.36	-10.66(4)	-10.92
5i3W-(5)	35	0.24	-8.15 (4)	-12.9
3TPP-(6)	41	0.23	-9.4 (4)	-9.28
4LC7-(7)	23	0.09	-2.15 (5)	-6.8

The drug-like properties when applying Lipinski's Rule of five, Veber Rule and MDDR Rule changed depending on functional groups and molecular weights. There is a good correlation between the Gibbs free energy (ΔG) calculated and the experimentally obtained values[46][54].

4. Conclusions

Preprints (www.preprints.org) | NOT PEER-REVIEWED | Posted: 10 November 2020 doi:10.20944/preprints202011.0292.v1

The parameters for successful drugs depend on the specificity and binding to the receptor, a 500 molecuar weight is preferred for good absorption, and a Kd value in the range of 1nM to 10nM , the potency depends on the specificity of binding (Asp) and increased hydrophobic binding residues are preferred, but this comes on the account of specificity, a balnce between specific binding and hydrphobicity should be maintained. The higher LE, the more promosing is the drug binding to a specific target.

The binding energy of drug to its target depends on a group of energies[55]; the first is desolvation energy needed to break the hydrogen bonds between inhibitor and solvent, then energy released upon binding of inhibitor to receptor and burying the inhibitor hydrophobic surface. Polar interactions and hydrophobic surface burial which depends on surface area (every $1Å^2$ of S.A releases approximately 25cal), see Table 6. The draw back, in the drugs under study, that is the limited surface area around 90 $Å^2$ for drugs to enter brain cells. Differences between calculated and actual ΔG values are due to imperfect H-bonds due to steric factors and distance factors which result in higher E-cost for desolvation.

Research on the mechanism of AD considered the BACE1 as a key enzyme which participates in the formation of Aβ, which broadly exists in the brains of AD patients. Compounds with peptidomimetic structures are effective in BACE1 inhibition according to experimental aspartic proteinase results in in vitro. Nevertheless, these kinds of BACE1 inhibitors did not perform well in pre-clinical trials due to their excessive number of hydrogen bond donors and acceptors, which increase the polarity and further lead to a lack of permeability across the BBB. Based on molecular dynamics and energy studies, the amino acid residues Asp228 and Asp32 in the BACE1 enzyme play an important role in the interactions between compounds and the enzyme. Furthermore, S1, S3, S2'and other pockets also exhibited a central role in binding with the BACE1 inhibitors. In the light of these studies, compounds with amino heterocycles were designed and synthesized. The presence of amino and aromatic rings maintained the inhibitory ability and decreased the polarity of the structure at the same time.

MM/PBSA energies are calculated for snapshots obtained by MD simulations. Variations are normally solved by calculating only interaction energies, studying many snapshots and using several independent simulations. It has been suggested that the calculations can be performed by using only minimized structures, but such results may depend on the starting structures. Finally, MM/GBSA when compared with other ligand binding methods, showed reasonable accuracy.

MM/GBSA is a popular method to calculate absolute binding affinities with a modest computational effort. Energy results from six well-defined terms. However, the dielectric constant, parameters for the non-polar energy, the radii used for the PB or GB calculations, and whether to include the entropy term and whether to perform MD simulations or minimizations. In practice, it typically gives results of intermediate quality, often better than docking and scoring, but worse than FEP, for example, $r^2 = 0.3$ for the whole PDB bind database, but $r^2 = 0.0$ -- 0.8 for individual proteins.

Acknowledgment: I would like to thank Professor J. Andrew McCammon, department of Biochemistry & Biophysics, UC-San Diego, USA for hosting me for a year in his group, and his generous support in providing all facilities including office space and access to GPU cluster. This work would not be possible without his support.

References

1. Gu, T.; Wu, W.Y.; Dong, Z.X.; Yu, S.P.; Sun, Y.; Zhong, Y.; Lu, Y.T.; Li, N.G. Development and Structural Modification of BACE1 Inhibitors. *Molecules* **2017**, *22*, doi:10.3390/molecules22010004.
2. Rombouts, F.J.R.; Alexander, R.; Cleiren, E.; De Groot, A.; Carpentier, M.; Dijkmans, J.; Fierens, K.; Masure, S.; Moechars, D.; Palomino-Schätzlein, M.; et al. Fragment Binding to β-Secretase 1 without Catalytic Aspartate Interactions Identified via Orthogonal Screening Approaches. *ACS Omega* **2017**, *2*, 685–697, doi:10.1021/acsomega.6b00482.
3. Ghosh, A.K.; Brindisi, M.; Tang, J. Developing $β$-secretase inhibitors for treatment of Alzheimer's disease. *J. Neurochem.* **2012**, *120*, 71–83.
4. Hong, L.; Koelsch, G.; Lin, X.; Wu, S.; Terzyan, S.; Ghosh, A.K.; Zhang, X.C.; Tang, J. Structure of the protease domain of memapsin 2 ($β$-secretase) complexed with inhibitor. *Science (80-.).* **2000**, *290*, 150–153.
5. Oehlrich, D.; Prokopcova, H.; Gijsen, H.J.M. The evolution of amidine-based brain penetrant BACE1 inhibitors. *Bioorg. Med. Chem. Lett.* **2014**, *24*, 2033–2045.

6. Malamas, M.S.; Erdei, J.; Gunawan, I.; Turner, J.; Hu, Y.; Wagner, E.; Fan, K.; Chopra, R.; Olland, A.; Bard, J.; et al. Design and synthesis of 5,5′-disubstituted aminohydantoins as potent and selective human β-secretase (BACE1) inhibitors. *J. Med. Chem.* **2010**, *53*, 1146–1158, doi:10.1021/jm901414e.
7. Steele, T.G.; Hills, I.D.; Nomland, A.A.; de León, P.; Allison, T.; McGaughey, G.; Colussi, D.; Tugusheva, K.; Haugabook, S.J.; Espeseth, A.S.; et al. Identification of a small molecule $β$-secretase inhibitor that binds without catalytic aspartate engagement. *Bioorg. Med. Chem. Lett.* **2009**, *19*, 17–20.
8. Ren, Z.; Tam, D.; Xu, Y.Z.; Wone, D.; Yuan, S.; Sham, H.L.; Cheung, H.; Regnstrom, K.; Chen, X.; Rudolph, D.; et al. Development of a novel β-secretase binding assay using the alphascreen platform. *J. Biomol. Screen.* **2013**, *18*, 695–704, doi:10.1177/1087057113482138.
9. Wang, E.; Sun, H.; Wang, J.; Wang, Z.; Liu, H.; Zhang, J.Z.H.; Hou, T. End-Point Binding Free Energy Calculation with MM/PBSA and MM/GBSA: Strategies and Applications in Drug Design. *Chem. Rev.* **2019**, *119*, 9478–9508, doi:10.1021/acs.chemrev.9b00055.
10. Srivastava, H.K.; Sastry, G.N. Molecular dynamics investigation on a series of HIV protease inhibitors: assessing the performance of MM-PBSA and MM-GBSA approaches. *J. Chem. Inf. Model.* **2012**, *52*, 3088–3098.
11. Narang, S.S.; Goyal, D.; Goyal, B. Inhibition of Alzheimer's amyloid-β42 peptide aggregation by a bi-functional bis-tryptoline triazole: key insights from molecular dynamics simulations. *J. Biomol. Struct. Dyn.* **2020**, *38*, 1598–1611, doi:10.1080/07391102.2019.1614093.
12. Lu, N.; Kofke, D.A. Accuracy of free-energy perturbation calculations in molecular simulation. II. Heuristics. *J. Chem. Phys.* **2001**, *115*, 6866–6875, doi:10.1063/1.1405449.
13. Veselovsky, A. V; Ivanov, A.S. Strategy of Computer-Aided Drug Design. *Curr. Drug Target -Infectious Disord.* **2003**, *3*, 33–40, doi:10.2174/1568005033342145.
14. Hou, T.; Wang, J.; Li, Y.; Wang, W. Assessing the Performance of the MM / PBSA and MM / GBSA Methods . I . The Accuracy of Binding Free Energy Calculations Based on Molecular Dynamics Simulations. *J. Chem. Inf. Model* **2010**, *51*, 69–82, doi:10.1021/ci100275a.
15. Temiz, N.A.; Trapp, A.; Prokopyev, O.A.; Camacho, C.J. Optimization of minimum set of protein--DNA interactions: a quasi exact solution with minimum over-fitting. *Bioinformatics* **2010**, *26*, 319–325.
16. Kirkwood, J.G. Statistical mechanics of fluid mixtures. *J. Chem. Phys.* **1935**, *3*, 300–313.
17. Srinivasan, J.; Miller, J.; Kollman, P.A.; Case, D.A. Continuum solvent studies of the stability of RNA hairpin loops and helices. *J. Biomol. Struct. Dyn.* **1998**, *16*, 671–682.
18. Kollman, P.A.; Massova, I.; Reyes, C.; Kuhn, B.; Huo, S.; Chong, L.; Lee, M.; Lee, T.; Duan, Y.; Wang, W.; et al. Calculating structures and free energies of complex molecules: combining molecular mechanics and continuum models. *Acc. Chem. Res.* **2000**, *33*, 889–97, doi:10.1021/ar000033j.

19. Kongsted, J.; Ryde, U. An improved method to predict the entropy term with the MM/PBSA approach. *J. Comput. Aided. Mol. Des.* **2009**, *23*, 63–71, doi:10.1007/s10822-008-9238-z.
20. Srinivasan, J.; Cheatham, T.E.; Cieplak, P.; Kollman, P.A.; Case, D.A. Continuum solvent studies of the stability of DNA, RNA, and phosphoramidate- DNA helices. *J. Am. Chem. Soc.* **1998**, *120*, 9401–9409.
21. Nidhi Singh1 and Arieh Warshel1 Absolute Binding Free Energy Calculations: On the Accuracy of Computational Scoring of Protein-ligand Interactions Nidhi. *Bone* **2008**, *23*, 1–7, doi:10.1038/jid.2014.371.
22. Vassar, R. BACE1 inhibitor drugs in clinical trials for Alzheimer's disease. *Alzheimer's Res. Ther.* **2014**, *6*, 1–14, doi:10.1186/s13195-014-0089-7.
23. Sliwoski, G.; Kothiwale, S.; Meiler, J.; Lowe, E.W. Computational Methods in Drug Discovery. **2014**, 334–395.
24. Ben-Shalom, I.Y.; Lin, C.; Kurtzman, T.; Walker, R.C.; Gilson, M.K. Simulating water exchange to buried binding sites. *J. Chem. Theory Comput.* **2019**, *15*, 2684–2691.
25. Pearlman, D.A.; Case, D.A.; Caldwell, J.W.; Ross, W.S.; Cheatham, T.E.; Steve, D.; Ferguson, D.; Seibel, G.; Kollman, P.; Cheatham III, T.E.; et al. AMBER, a package of computer programs for applying molecular mechanics, normal mode analysis, molecular dynamics and free energy calculations to simulate the structural and energetic properties of molecules. *Comput. Phys. Commun.* **1995**, *91*, 1–41, doi:10.1016/0010-4655(95)00041-D.
26. How to Cite Amber. *Am. Ethnol.* **2020**, *47*, 209, doi:10.1111/amet.12914.
27. Götz, A.W.; Williamson, M.J.; Xu, D.; Poole, D.; Le Grand, S.; Walker, R.C. Routine Microsecond Molecular Dynamics Simulations with AMBER on GPUs. 1. Generalized Born. *J. Chem. Theory Comput.* **2012**, *8*, 1542–1555, doi:10.1021/ct200909j.
28. Maier, J.A.; Martinez, C.; Kasavajhala, K.; Wickstrom, L.; Hauser, K.E.; Simmerling, C. ff14SB: Improving the Accuracy of Protein Side Chain and Backbone Parameters from ff99SB. *J. Chem. Theory Comput.* **2015**, *11*, 3696–3713, doi:10.1021/acs.jctc.5b00255.
29. Ponder, J.W.; Case, D.A. Force fields for protein simulations. *Adv. Protein Chem.* **2003**, *66*, 27–85, doi:10.1016/S0065-3233(03)66002-X.
30. Rother, K. Introduction to PyMOL. *Methods Mol. Biol. Clift. Nj* **2005**, *635*, 0–32, doi:10.1213/ANE.0b013e3181e9c3f3.
31. Ross Walker Sishi Tang Antechamber Tutorial. **2005**, 1–7.
32. Wang, J.M.; Wolf, R.M.; Caldwell, J.W.; Kollman, P. a; Case, D. a Development and testing of a general amber force field. *J. Comput. Chem.* **2004**, *25*, 1157–1174, doi:10.1002/jcc.20035.
33. Jorgensen, W.L.; Chandrasekhar, J.; Madura, J.D.; Impey, R.W.; Klein, M.L. Comparison of simple potential functions for simulating liquid water. *J. Chem. Phys.* **1983**, *79*, 926–935, doi:10.1063/1.445869.
34. Essmann, U.; Perera, L.; Berkowitz, M.L.; Darden, T.; Lee, H.; Pedersen, L.G. A smooth particle mesh Ewald method. *J. Chem. Phys.* **1995**, *103*, 8577–8593,

doi:10.1063/1.470117.

35. Kräutler, V.; Van Gunsteren, W.F.; Hünenberger, P.H. A fast SHAKE algorithm to solve distance constraint equations for small molecules in molecular dynamics simulations. *J. Comput. Chem.* **2001**, *22*, 501–508.
36. Berendsen, H.J.C.; Postma, J.P.M.; Van Gunsteren, W.F.; Dinola, A.; Haak, J.R. Molecular dynamics with coupling to an external bath. *J. Chem. Phys.* **1984**, *81*, 3684–3690, doi:10.1063/1.448118.
37. Cerutti, D.S.; Duke, R.; Freddolino, P.L.; Fan, H.; Lybrand, T.P. A Vulnerability in Popular Molecular Dynamics Packages Concerning Langevin and Andersen Dynamics. *J. Chem. Theory Comput.* **2008**, *4*, 1669–1680, doi:10.1021/ct8002173.
38. Miller, B.R.; Mcgee, T.D.; Swails, J.M.; Homeyer, N.; Gohlke, H.; Roitberg, A.E. MMPBSA.py: An E ffi cient Program for End-State Free Energy Calculations. *J. Chem. Theory Comput.* **2012**, *8*, 3314–3321.
39. Genheden, S.; Ryde, U. The MM/PBSA and MM/GBSA methods to estimate ligand-binding affinities. *Expert Opin. Drug Discov.* **2015**, *10*, 449–461, doi:10.1517/17460441.2015.1032936.
40. Wang, J.; Morin, P.; Wang, W.; Kollman, P. a Use of MM-PBSA in reproducing the binding free energies to HIV-1 RT of TIBO derivatives and predicting the binding mode to HIV-1 RT of efavirenz by docking and MM-PBSA. *J. Am. Chem. Soc.* **2001**, *123*, 3986–3994.
41. Hermansson, A. Calculating Ligand-Protein Binding Energies from Molecular Dynamics Simulations - Thesis in Physical Chemistry. **2015**.
42. Roe, D.R.; Cheatham III, T.E. PTRAJ and CPPTRAJ: software for processing and analysis of molecular synamics trajectory data. *J Chem Theory Com* **2013**, *9*, 3084–3095, doi:10.1021/ct400341p.
43. Lill, M.A.; Thompson, J.J. Solvent interaction energy calculations on molecular dynamics trajectories: Increasing the efficiency using systematic frame selection. *J. Chem. Inf. Model.* **2011**, *51*, 2680–2689, doi:10.1021/ci200191m.
44. Galindo-Murillo, R.; Roe, D.R.; Cheatham, T.E. Convergence and reproducibility in molecular dynamics simulations of the DNA duplex d(GCACGAACGAACGAACGC). *Biochim. Biophys. Acta - Gen. Subj.* **2015**, *1850*, 1041–1058, doi:10.1016/j.bbagen.2014.09.007.
45. Galindo-Murillo, R.; Roe, D.R.; Cheatham, T.E. On the absence of intrahelical DNA dynamics on the μs to ms timescale. *Nat. Commun.* **2014**, *5*, doi:10.1038/ncomms6152.
46. BINDING constants Available online: http://www.bindingdb.org/pdb/1o86.
47. binding MOAD Available online: http://bindingmoad.org/.
48. RCSB.
49. Pajouhesh, H.; Lenz, G.R. Medicinal chemical properties of successful central nervous system drugs. *NeuroRx* **2005**, *2*, 541–553, doi:10.1602/neurorx.2.4.541.
50. Manuscript, A.; Nanobiomaterials, B. NIH Public Access. **2013**, *6*, 866–877, doi:10.1021/nn300902w.Release.
51. H, I. Lipophilic Ligand Efficiency as a Useful Metric in Hit and Lead Optimization. *J. Med. Chem. Drug Des.* **2019**, *2*, 9–10, doi:10.16966/2578-9589.112.

 doi:10.20944/preprints202011.0292.v1

52. Kenny, P.W. The nature of ligand efficiency. *J. Cheminform.* **2019**, *11*, 1–18, doi:10.1186/s13321-019-0330-2.
53. Hopkins, A.L.; Keserü, G.M.; Leeson, P.D.; Rees, D.C.; Reynolds, C.H. The role of ligand efficiency metrics in drug discovery. *Nat. Rev. Drug Discov.* **2014**, *13*, 105–121, doi:10.1038/nrd4163.
54. Wang, C.; Nguyen, P.H.; Pham, K.; Huynh, D.; Le, T.B.N.; Wang, H.; Ren, P.; Luo, R. Calculating protein-ligand binding affinities with MMPBSA: Method and error analysis. *J. Comput. Chem.* **2016**, *37*, doi:10.1002/jcc.24467.
55. Li, S.; Zhao, H.; Li, J.; Hao, J.; Yu, H. A series of molecular modeling techniques to reveal selective mechanisms of inhibitors to β-Site amyloid precursor protein cleaving enzyme 1 (BACE1) and β-site amyloid precursor protein cleaving enzyme 2 (BACE2). *J. Biomol. Struct. Dyn.* **2020**, *0*, 1–14, doi:10.1080/07391102.2020.1754917.

Supplementary Materials: The following are available online at www.mdpi.com/xxx/s1, Figure S1: title, Table Figure S1 Binding mode of Inhibitor 1 in 5i3x different views

Prediction of Drug Potencies of BACE1 inhibitors: A molecular Dynamics simulation and MM_GB(PB)SA Scoring

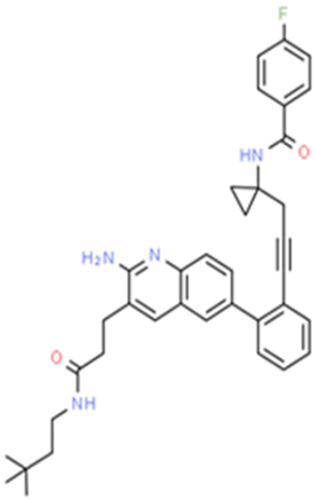

Preprints (www.preprints.org) | NOT PEER-REVIEWED | Posted: 10 November 2020 doi:10.20944/preprints202011.0292.v1

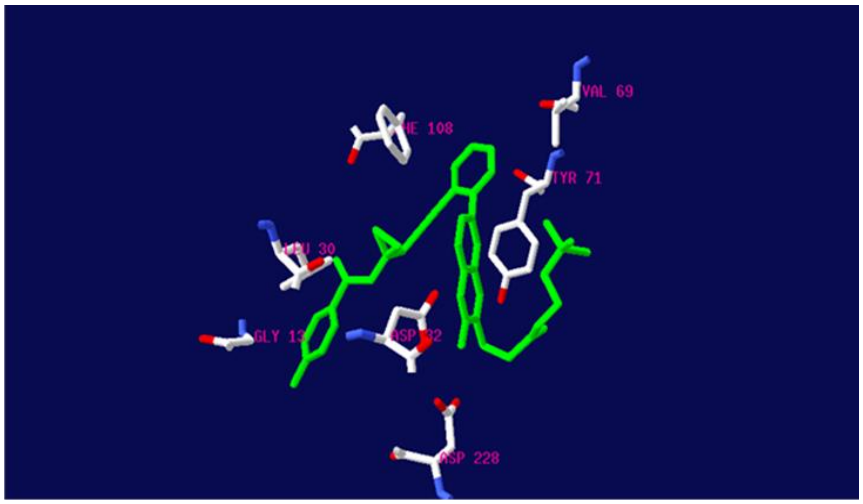

FigureS2: : Different views of binding of inhibitor 4 in 5i3v

5i3V

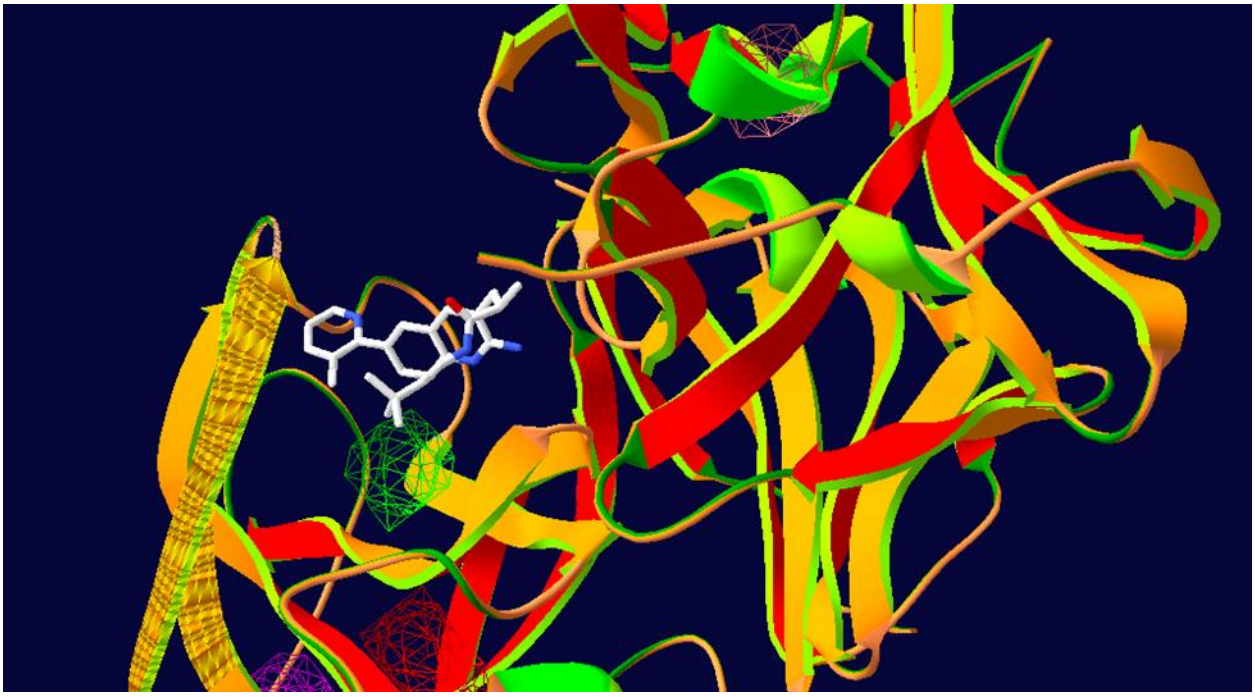

Preprints (www.preprints.org) | NOT PEER-REVIEWED | Posted: 10 November 2020 doi:10.20944/preprints202011.0292.v1

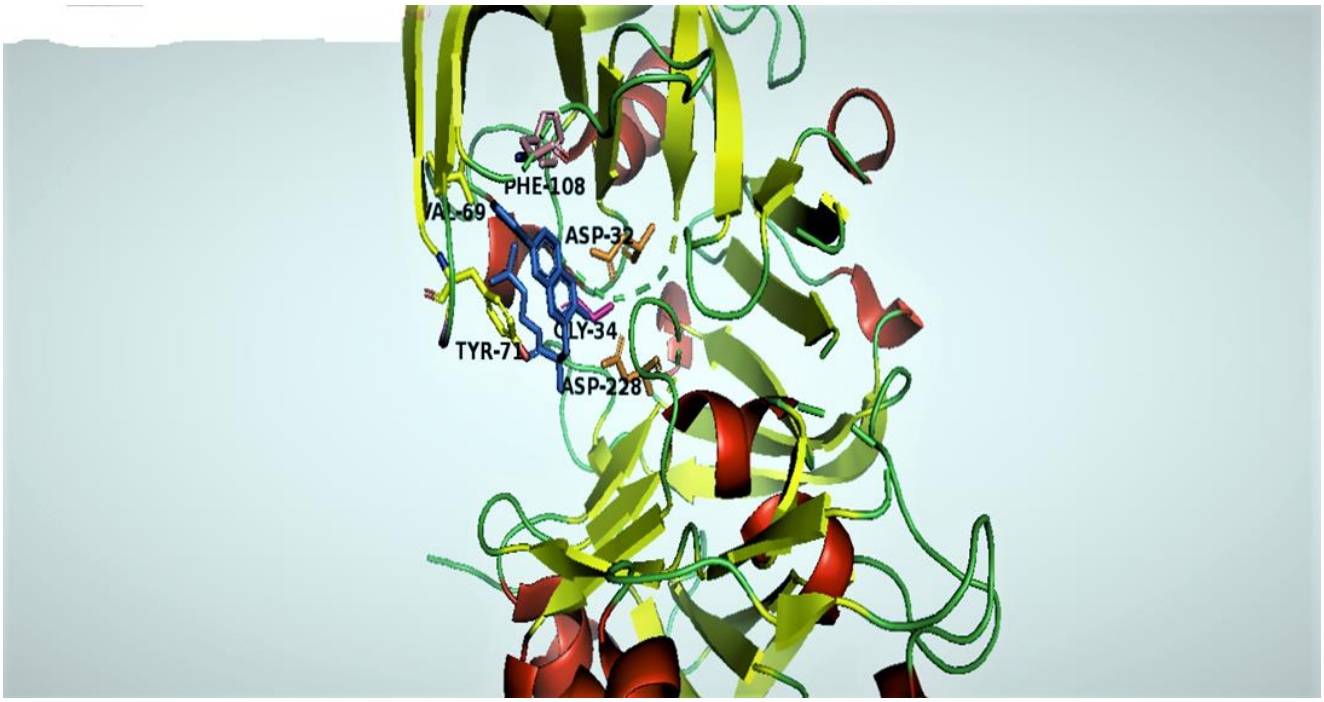

Figure S3: Binding mode of Inhibitor 6 in 4LC7 Different views

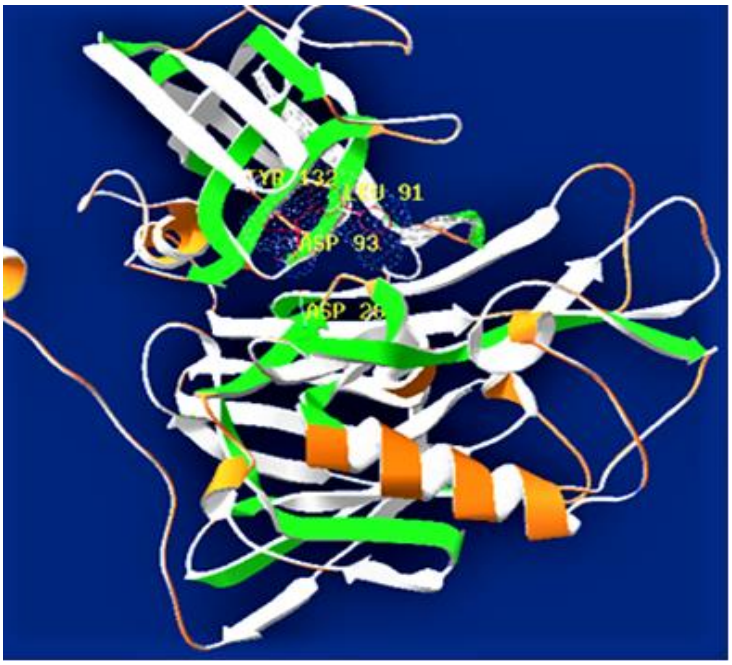

Preprints (www.preprints.org) | NOT PEER-REVIEWED | Posted: 10 November 2020 doi:10.20944/preprints202011.0292.v1

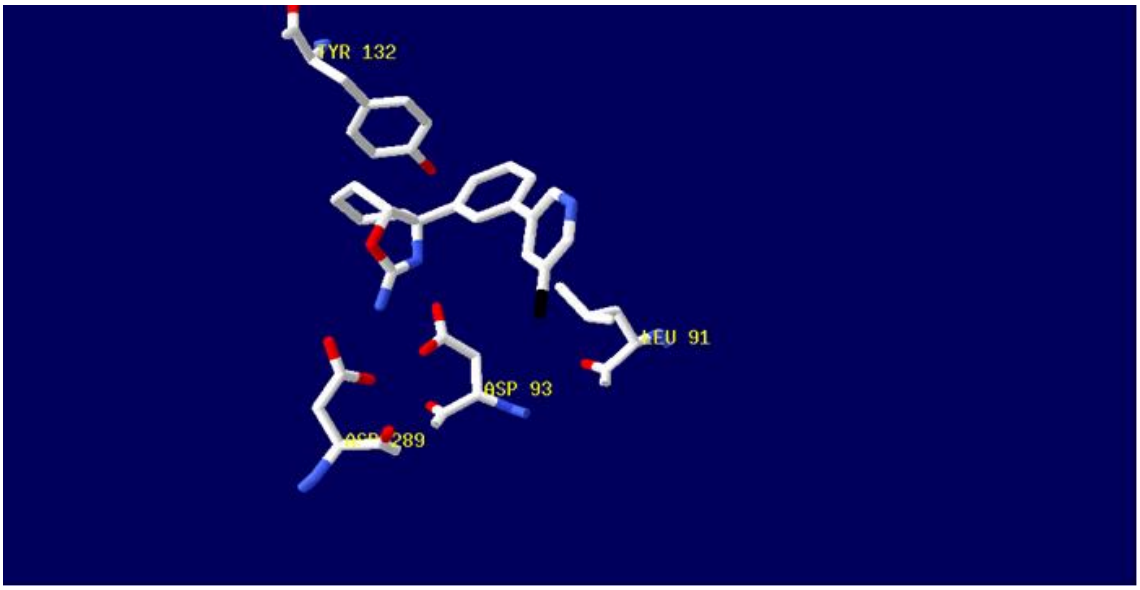

FigureS4: protein view of inhibitor 7 in 3TPP

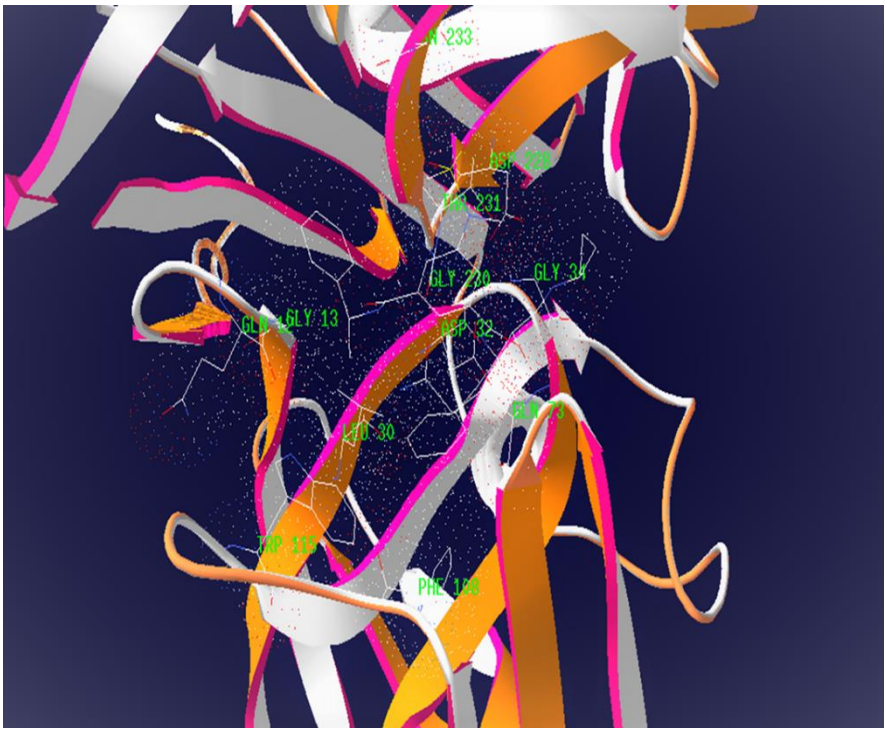

Preprints (www.preprints.org) | NOT PEER-REVIEWED | Posted: 10 November 2020 doi:10.20944/preprints202011.0292.v1

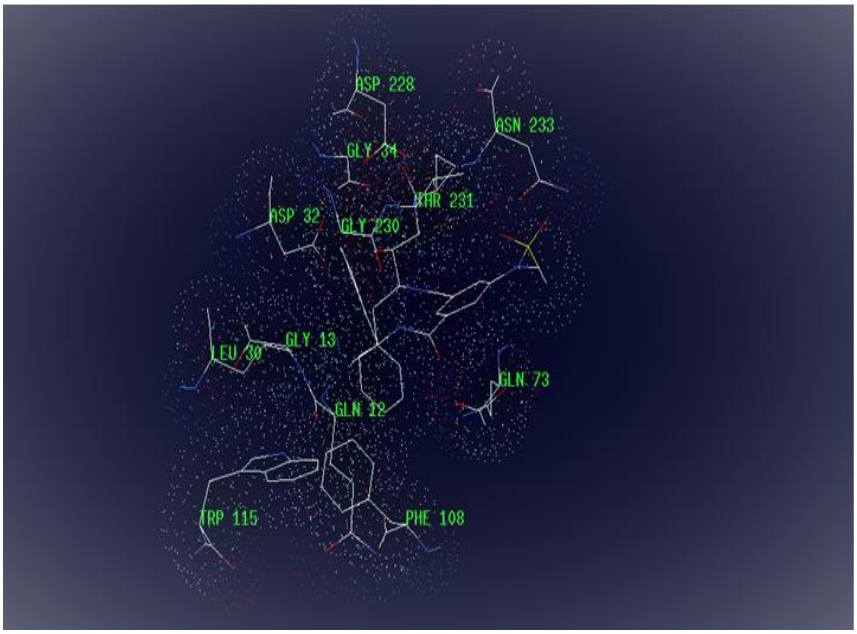

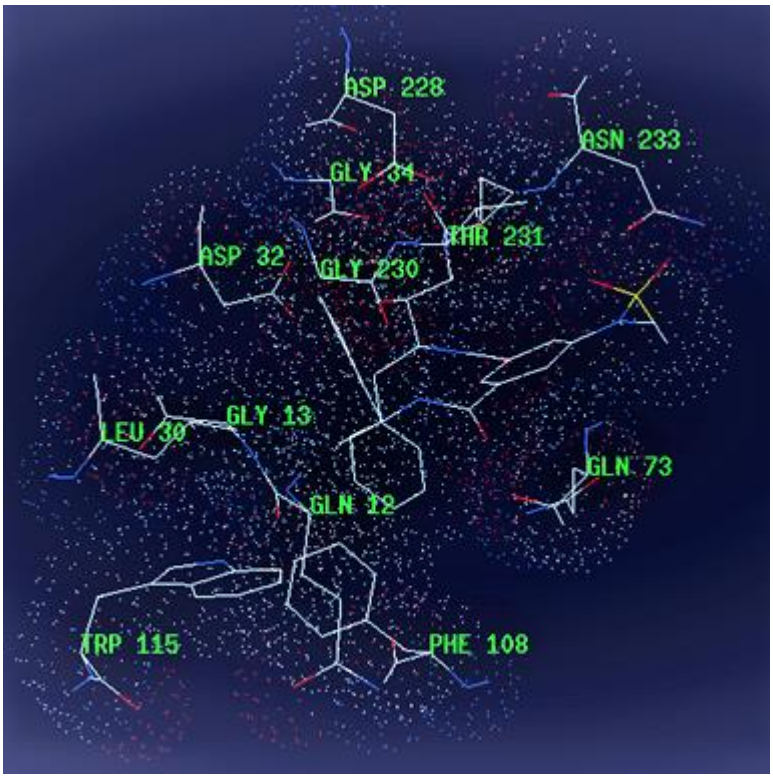

FigureS5 surface areas of inhibitors and the BACE1 surface

Preprints (www.preprints.org) | NOT PEER-REVIEWED | Posted: 10 November 2020 doi:10.20944/preprints202011.0292.v1

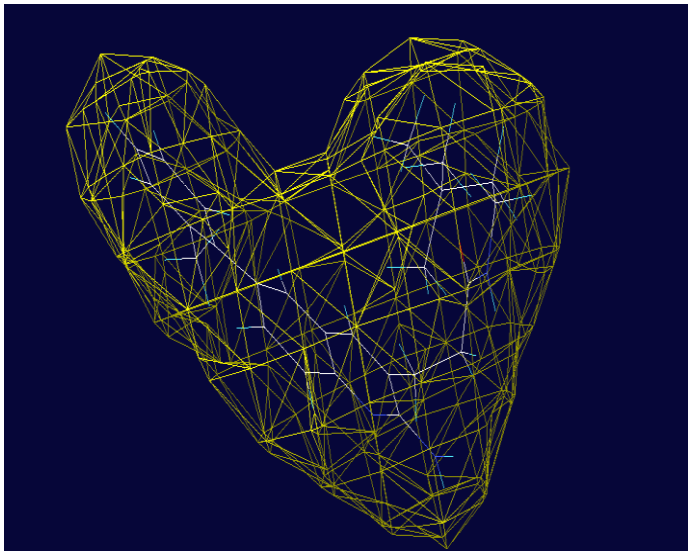

6BS-30.5

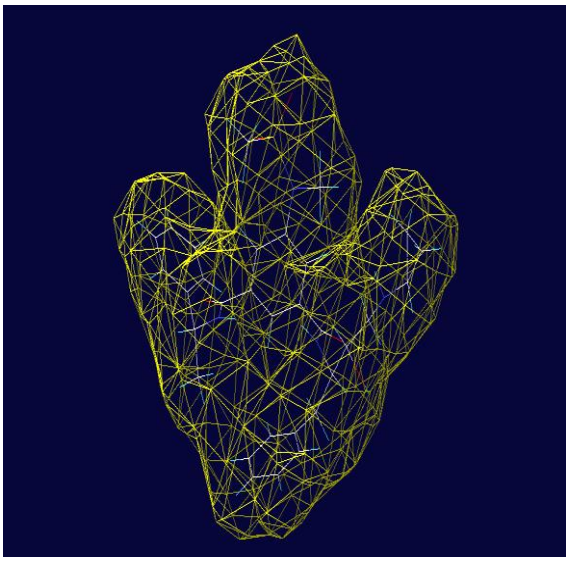

5HA -35.6

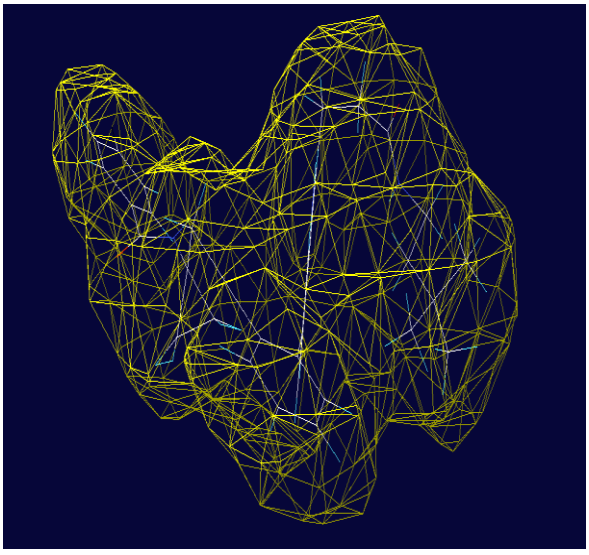

68J

Preprints (www.preprints.org) | NOT PEER-REVIEWED | Posted: 10 November 2020 doi:10.20944/preprints202011.0292.v1

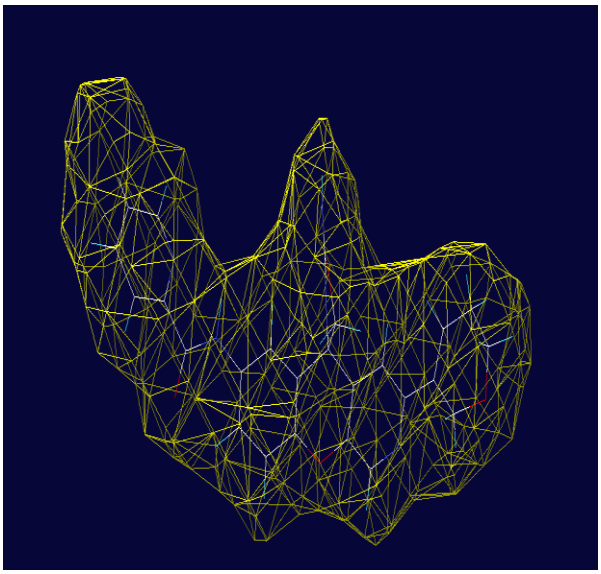

68K

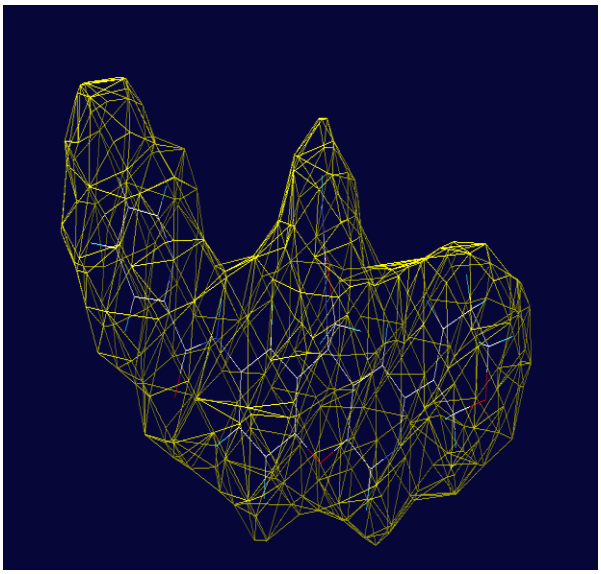

68L

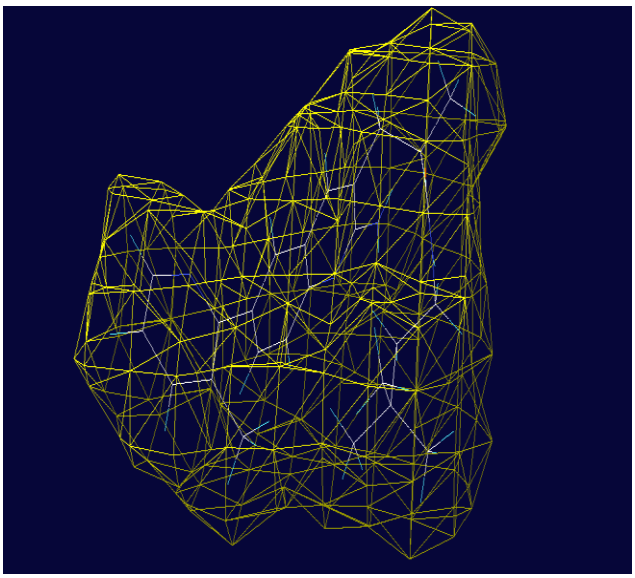

Preprints (www.preprints.org) | NOT PEER-REVIEWED | Posted: 10 November 2020 doi:10.20944/preprints202011.0292.v1

68M

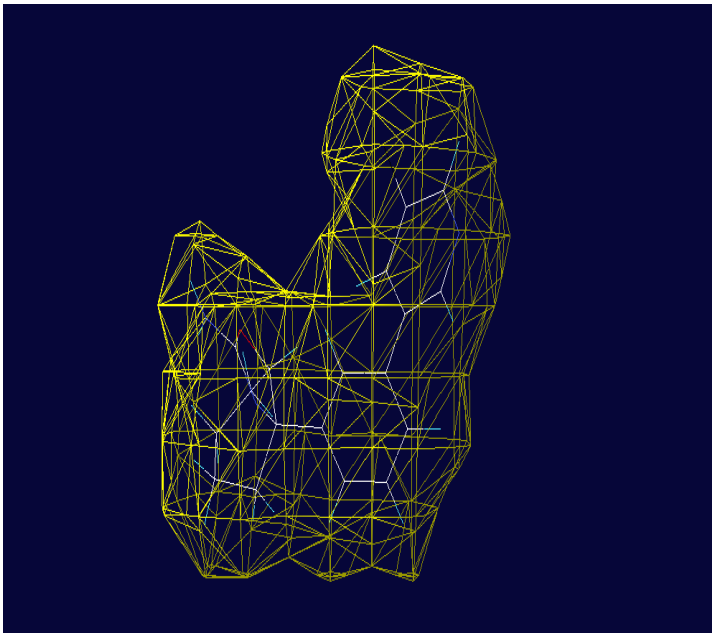

1WP

Figure S6: Views of Inhibitor 3 binding protein view (5ie1)

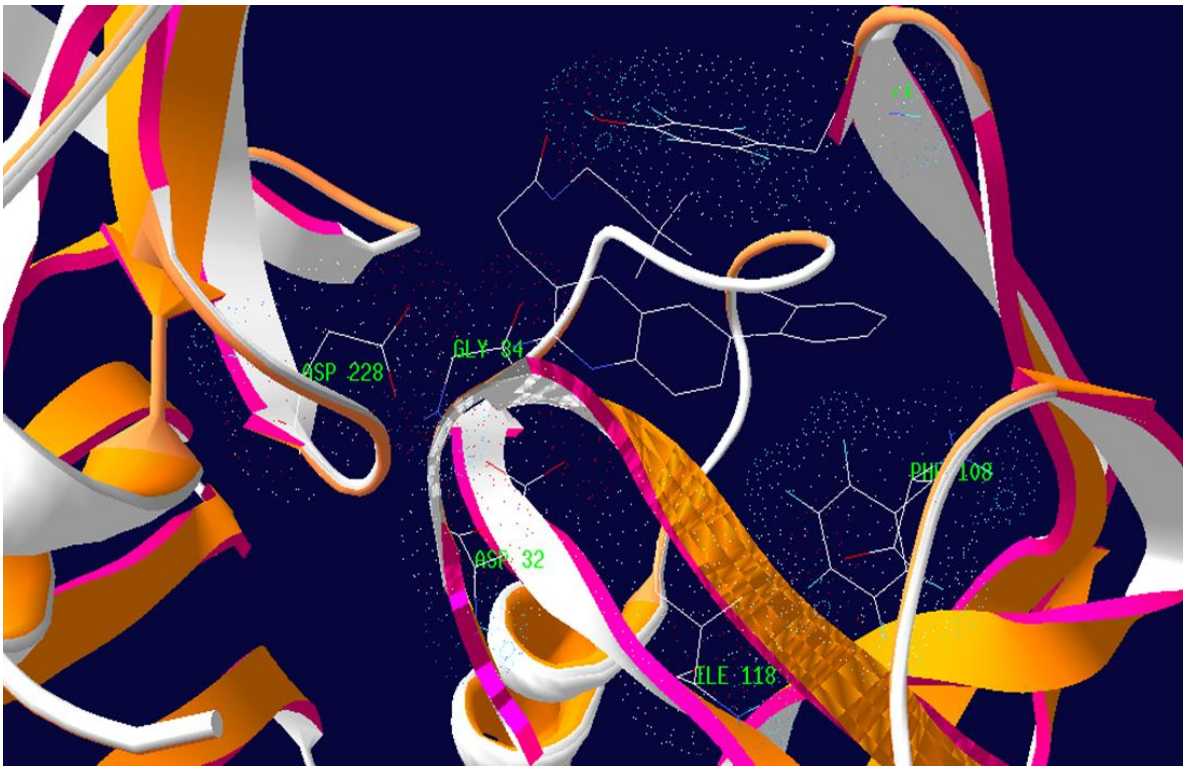

Figure S7: views of inhibitor 2 to BACE1 (5i3Y)

Preprints (www.preprints.org) | NOT PEER-REVIEWED | Posted: 10 November 2020 doi:10.20944/preprints202011.0292.v1

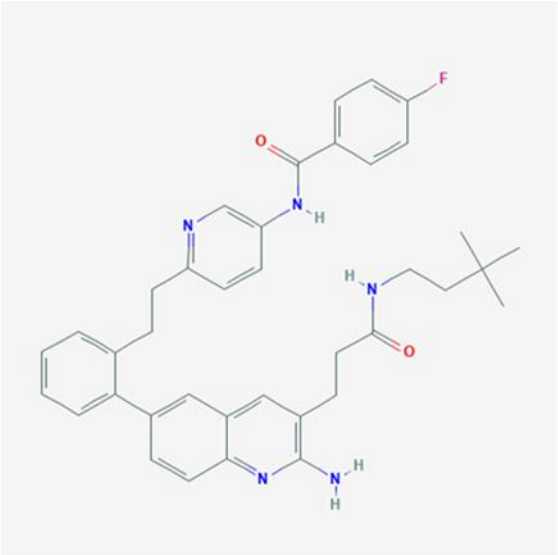

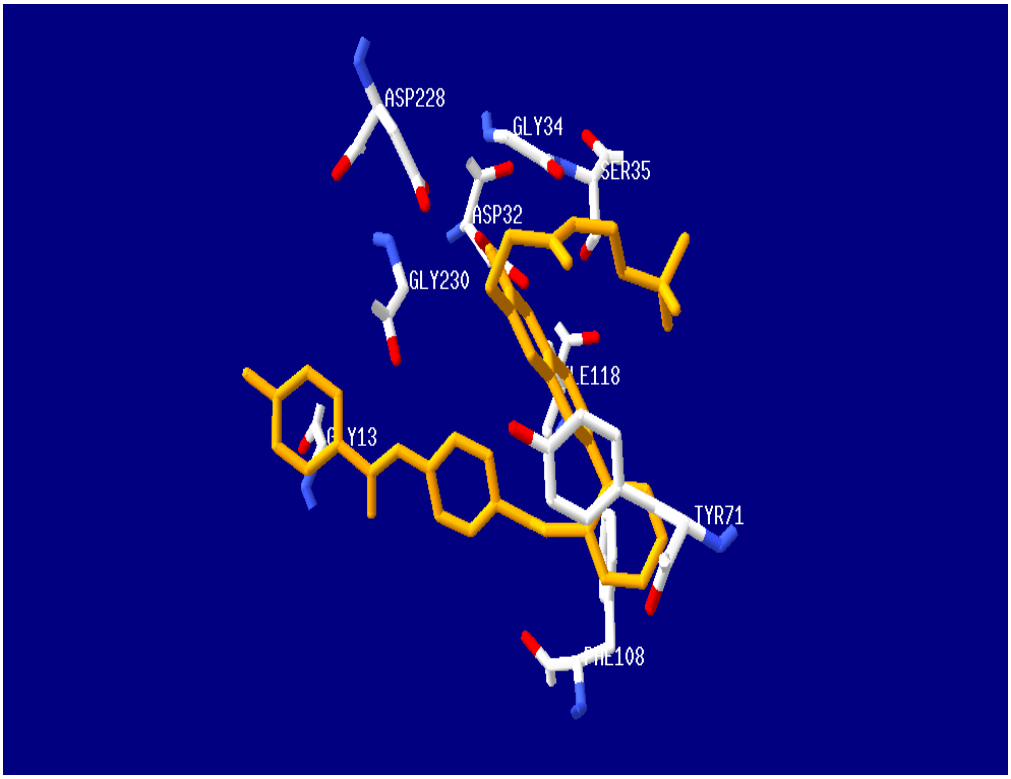

Figure S8: 5i3W binding of inhibitor 5 to BACE1

Preprints (www.preprints.org) | NOT PEER-REVIEWED | Posted: 10 November 2020 doi:10.20944/preprints202011.0292.v1

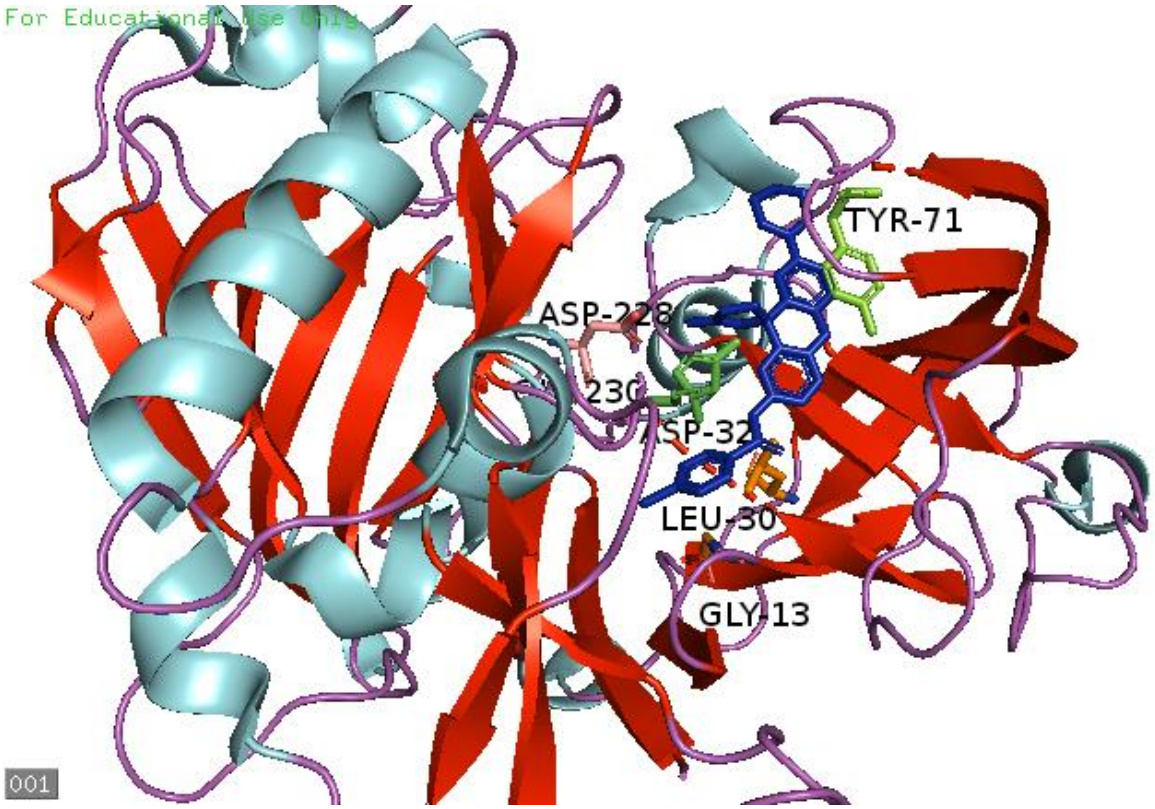

Figure 69: : shows a dendogram (cluster trees) of the BACE1-Inhibitor in 5i3X

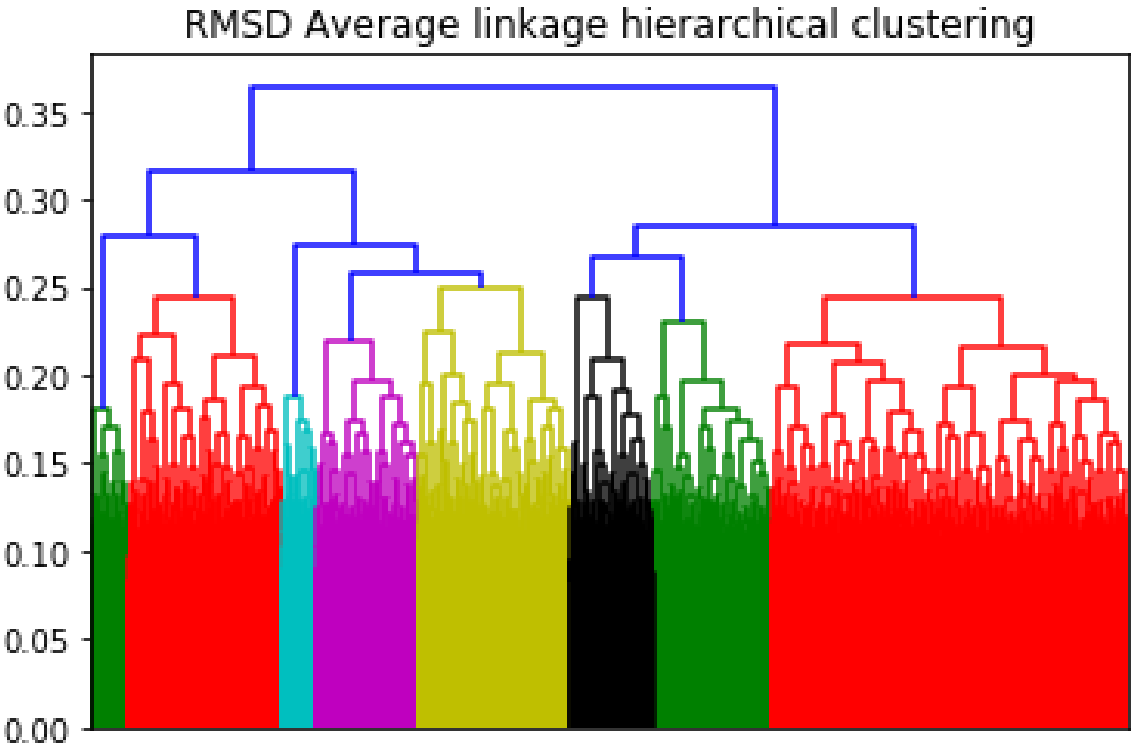

Figure: shows a dendogram (cluster trees) of the BACE1-Inhibitor in 5i3X complex employing RMSD. The Principal component analysis (PCA) technique transformed the trajectory frames into a set of

 doi:10.20944/preprints202011.0292.v1

orthogonal vectors (PCs) to help explain the variance in coordinate space. PCs represent certain modes of motion with the first PC shows the largest variance and the dominant motion in the system. This helped to gain insight into the dynamics of the system (the actual motion of the system) throughout the course of a simulation which is a combination of the